



HAL
open science

The quasi-universality of nestedness in the structure of quantitative plant-parasite interactions

Benoît Moury, Jean-Marc Audergon, Sylvie Baudracco-Arnas, Safa Ben Krima, François Bertrand, Nathalie Boissot, Mireille Buisson, Valérie Caffier, Melissa Cantet, Sylvia Chanéac, et al.

► To cite this version:

Benoît Moury, Jean-Marc Audergon, Sylvie Baudracco-Arnas, Safa Ben Krima, François Bertrand, et al.. The quasi-universality of nestedness in the structure of quantitative plant-parasite interactions. 2021. hal-03169796

HAL Id: hal-03169796

<https://hal.inrae.fr/hal-03169796>

Preprint submitted on 23 Jun 2021

HAL is a multi-disciplinary open access archive for the deposit and dissemination of scientific research documents, whether they are published or not. The documents may come from teaching and research institutions in France or abroad, or from public or private research centers.

L'archive ouverte pluridisciplinaire **HAL**, est destinée au dépôt et à la diffusion de documents scientifiques de niveau recherche, publiés ou non, émanant des établissements d'enseignement et de recherche français ou étrangers, des laboratoires publics ou privés.



Distributed under a Creative Commons Attribution - NonCommercial - NoDerivatives 4.0 International License

1 The quasi-universality of nestedness in the structure of quantitative plant- 2 parasite interactions

3

4 Moury Benoît¹, Audergon Jean-Marc², Baudracco-Arnas Sylvie³, Ben Krima Safa⁴, Bertrand François⁵,
5 Boissot Nathalie², Buisson Mireille⁶, Caffier Valérie⁷, Cantet Mélissa^{2*}, Chanéac Sylvia⁸, Constant
6 Carole⁹, Delmotte François¹⁰, Dogimont Catherine², Doumayrou Juliette¹⁵, Fabre Frédéric¹⁰, Fournet
7 Sylvain¹¹, Grimault Valérie¹², Jaunet Thierry¹³, Justafré Isabelle¹⁴, Lefebvre Véronique², Losdat Denis¹⁵,
8 Marcel Thierry⁴, Montarry Josselin¹¹, Morris Cindy E.¹, Omrani Mariem^{1,2}, Paineau Manon¹⁰, Perrot
9 Sophie¹², Pilet-Nayel Marie-Laure¹¹, Ruellan Youna²

10

11 ¹Pathologie Végétale, INRAE, 84140 Montfavet, France

12 ²GAFL, INRAE, 84140, Montfavet, France

13 ³Laboratoires ASL, 755 chemin de Meinajaries, 84140 Montfavet, France

14 ⁴University of Paris-Saclay, INRAE, AgroParisTech, UMR BIOGER, 78850 Thiverval-Grignon, France

15 ⁵Bayer Seeds SAS, Chemin de Roquemartine Mas Lamy, 13670, Saint-Andiol, France

16 ⁶GAUTIER SEMENCES, Route d'Avignon, 13630 Eyragues, France

17 ⁷Univ Angers, Institut Agro, INRAE, IRHS, SFR QUASAV, 49000 Angers, France

18 ⁸TAKII FRANCE SAS, 660 Chemin de la Crau, 13630 EYRAGUES, France.

19 ⁹Sakata Vegetables Europe, Domaine de Sablas, rue du moulin, 30620 Uchaud, France

20 ¹⁰SAVE, INRAE, Bordeaux Sciences Agro, ISVV, 33140 Villenave d'Ornon, France

21 ¹¹IGEPP, INRAE, Institut Agro, Univ. Rennes, 35653 Le Rheu, France

22 ¹²GEVES, 25 rue Georges Morel, CS 900024, 49071 Beaucouzé, France

23 ¹³HM.Clause, 1 chemin du Moulin des Ronzières, 49800 La Bohalle, France

24 ¹⁴Vilmorin, Mas Pazac, 30210 Ledenon, France

25 ¹⁵RIJK ZWAAN France, La Vernède, 30390 Aramon, France

26

27 *present address: Bayer Seeds SAS, Chemin de Roquemartine Mas Lamy, 13670, Saint-Andiol, France

28 [§]present address : Syngenta Seeds B.V., Westeinde 62, P.O. box 2, Enkhuizen 1600 AA, The
29 Netherlands

30

31 **Abstract**

32 Understanding the relationships between host range and pathogenicity for parasites, and between
33 the efficiency and scope of immunity for hosts are essential to implement efficient disease control
34 strategies. In the case of plant parasites, most studies have focused on describing qualitative
35 interactions and a variety of genetic and evolutionary models has been proposed in this context.
36 Although plant quantitative resistance benefits from advantages in terms of durability, we presently
37 lack models that account for quantitative interactions between plants and their parasites and the
38 evolution of these interactions. Nestedness and modularity are important features to unravel the
39 overall structure of host-parasite interaction matrices. Here, we analysed these two features on 32
40 matrices of quantitative pathogenicity trait data gathered from 15 plant-parasite pathosystems
41 consisting of either annual or perennial plants along with fungi or oomycetes, bacteria, nematodes,
42 insects and viruses. The performance of several nestedness and modularity algorithms was evaluated
43 through a simulation approach, which helped interpretation of the results. We observed significant
44 modularity in only six of the 32 matrices, with two or three modules detected. For three of these
45 matrices, modules could be related to resistance quantitative trait loci present in the host. In
46 contrast, we found high and significant nestedness in 30 of the 32 matrices. Nestedness was linked to
47 other properties of plant-parasite interactions. First, pathogenicity trait values were explained in
48 majority by a parasite strain effect and a plant accession effect, with no parasite-plant interaction
49 term. Second, correlations between the efficiency and scope of the resistance of plant genotypes,
50 and between the host range breadth and pathogenicity level of parasite strains were overall positive.
51 This latter result questions the efficiency of strategies based on the deployment of several
52 genetically-differentiated cultivars of a given crop species in the case of quantitative plant immunity.

53

54 **Keywords**

55 Plant resistance, pathogenicity, plant parasite, bipartite network, nestedness, modularity

56

57 Introduction

58 The effectiveness of strategies of disease control based on host immunity depends on the underlying
59 capabilities of hosts to resist infection, of parasites to overcome this resistance and on the potential
60 of these traits to evolve. Parasites and hosts can be specialists or generalists in, respectively, their
61 capacity to infect and their immunity. Confronting multiple genotypes of a parasite with multiple
62 genotypes of a host reveals their interaction patterns, *i.e.* the magnitude and arrangement of their
63 mutual specialization or generalism, which gives insights into the underlying genetic bases of these
64 characters and allows implementing strategies of disease management based on host diversification.

65 Importantly, the word “interaction” has different meanings in this context. In ecology, interactions
66 between hosts and parasites are the effects that each of these two categories of living organisms
67 have on each other. These host-parasite interactions can involve molecular interactions, which are
68 attractive or repulsive forces between molecules, for example between parasite elicitors or effectors
69 and host receptors. Finally, quantitative pathogenicity traits can be analysed thanks to statistical
70 models that include, or not, a significant interaction between variables representing hosts and
71 parasites. In the latter acception, “interaction” means that the model departs significantly from a
72 purely additive model, including only a parasite effect and a host effect. Statistical interactions are
73 used in the context of quantitative data and linear regression models, but not for qualitative binary
74 data.

75 The structure of any host-parasite interaction can be represented as a matrix where columns
76 correspond to host genotypes (either inbred lines, clones or F₁ hybrids) and rows to parasite strains
77 (either isolates, clones or populations depending on the considered parasite). Each cell in the matrix
78 indicates the result of the pairwise confrontation between the corresponding host genotype and
79 parasite strain. Qualitative interactions generate binary matrices with 1 and 0 grades, which
80 correspond to successful and unsuccessful infections. Nestedness and modularity are two
81 quantitative properties that reveal non-random distributions of 1 and 0 grades in such matrices
82 (Weitz et al. 2013). Nestedness measures the tendency of the hosts of a parasite to have a
83 hierarchical organization, where the set of hosts of a given parasite (a species or a genotype) is a
84 subset (respectively superset) of that of the parasites of broader (respectively narrower) host ranges.
85 Here, the breadth of the host range of a given parasite is defined as the percentage of host species
86 (or genotypes) that are infected by this parasite. The same tendency is observed for host immunity
87 (Fig. 1A): the set of parasites that are controlled by the immunity of a given host is a subset
88 (respectively superset) of that of hosts with broader (respectively narrower) scopes of resistance.
89 Here, the scope of the resistance of a given host is defined as the percentage of parasite species (or
90 strains) that are targeted by this resistance.

91 Modularity measures the strength by which the matrix can be divided into several modules grouping
92 subsets of hosts and parasites characterized by successful infections, infections being rare for hosts
93 and parasites belonging to different modules (Fig. 1B). Depending on the genetic, evolutionary and
94 mechanistic patterns of host-parasite interactions, contrasted scores for nestedness and modularity
95 are expected.

96 Three main models of host-parasite interactions have been proposed for qualitative plant-parasite
97 interactions (Fig. 1C to F; see Thrall et al. 2016 for details). These models represent the mutual
98 specialization of hosts and parasites in terms of underlying molecular mechanisms, genetic
99 determinism and coevolution pattern. Each one generates a specific structural pattern in the
100 corresponding interaction matrix. Historically, the first model was the gene-for-gene (GFG) model
101 proposed to describe interactions between crop plants and their parasites, based on genetic studies
102 of flax and rust (Flor 1956). In this model, plant immunity is inducible and requires recognition of the
103 parasite by its host. Recognition occurs between a host receptor and a parasite elicitor, each of them
104 being encoded by a single gene. The loss or alteration of the elicitor in the parasite or the absence of
105 a cognate resistance allele in its host results in infection. Here, the word 'elicitor' is used in the broad
106 sense of a parasite component triggering plant defenses, and thus includes effectors and avirulence
107 factors (Bent and Mackey 2007). This model is coherent with dominant resistance that involves plant
108 proteins containing nucleotide-binding and leucine-rich-repeat domains as receptors, and that
109 mounts hypersensitive reactions (programmed cell death) upon recognition of various kinds of
110 parasite elicitors. In this system, a parasite strain may have universal infectivity, *i.e.* may be able to
111 infect all host genotypes, if it lacks all the elicitors that correspond to the host resistance factors.
112 Accordingly, the matrix has a global nested pattern, with partial or complete overlap of the host
113 ranges of the parasite strains and of the resistance spectra of the host genotypes (Fig. 1C,D).
114 Secondly, the matching-allele (MA) model was proposed to describe the self/non-self recognition
115 system of invertebrate immunity (Grosberg and Hart 2000). In that case, infectivity requires a specific
116 match between the host genotype and the parasite strain and, accordingly, universal infectivity is
117 impossible. The corresponding host-parasite matrix has a modular structure. Cross-infections are
118 frequent between hosts and parasites belonging to the same module but rare between hosts and
119 parasites belonging to distinct modules. In extreme cases of specialization, modules can be as small
120 as a single host-parasite pair (Fig. 1E). Mechanistically, this model is coherent with recessive plant
121 resistance to viruses mediated by eukaryotic translation initiation factors (e.g. Sacristán and García-
122 Arenal 2008) and with necrotrophic fungi which secrete elicitors of programmed cell death that
123 increase plant susceptibility by allowing the fungus to feed on dying cells (Peters et al. 2019). In the
124 context of plant necrotrophic parasites, this model is also confusingly named 'inverse gene-for-gene'

125 (Peters et al. 2019). Thirdly, the inverse-matching-allele (IMA) model was proposed to reflect the
126 adaptive immune system of vertebrates, where the host resists through recognition of the parasite
127 and infections occur when the parasite mismatches the host (Kidner and Moritz 2013; Thrall et al.
128 2016). The IMA model was defined in the context of multi-allelic series of resistance and
129 pathogenicity genes. Mechanistically very similar to the GFG model, it assumes that recognition
130 between host and parasite genotypes is highly specific. The corresponding host-parasite matrix is
131 therefore similar to the matching-allele model but with 0 and 1 grades replaced by 1 and 0 grades,
132 respectively (Fig. 1F). Hence, a modular pattern is the expected result when immunity levels (instead
133 of the degree of pathogenicity) are indicated in the matrix.

134 The distinguishing feature of the genetic models described above is that they describe qualitative
135 binary interactions, where each host-parasite pair is characterized by its compatibility or non-
136 compatibility. Models that describe quantitative host-parasite interactions are rare and their
137 adequacy to represent empirical data have not been extensively tested (Lambrechts 2010; Wang et
138 al. 2018). Analysis of quantitative plant immunity has mostly been confined to the framework of
139 quantitative genetics and QTL (quantitative trait loci) mapping. These methods usually assume that
140 resistance is determined by the additive effect of QTLs. More complex effects (dominance, epistasis)
141 are rarely considered (Gallois et al. 2018). Furthermore, there are few studies of quantitative
142 genetics and QTL mapping of parasite pathogenicity traits, especially in the case of plant parasites
143 (Wang et al. 2018). Most importantly, these few analyses were conducted either with a set of hosts
144 confronted to a single parasite or with a set of parasites confronted to a single host. In any case,
145 there is a clear need for new models describing quantitative host-parasite interactions while properly
146 accounting for the variability of both partners (Lambrechts 2010; Bartoli and Roux 2017). Moreover,
147 previous work has shown that the outcome of analysis of matrix structure is markedly impacted
148 when quantitative interactions are considered. Quantitative data are especially influencing the
149 significance of nestedness (Staniczenko et al. 2013).

150 These considerations motivated us to conduct a comprehensive analysis of the nestedness and
151 modularity of interaction matrices to deepen our knowledge in the specialization between plants and
152 diverse parasites using quantitative data. The objectives of this work are (i) to assess the
153 performance of available algorithms to identify nested and modular patterns in matrices of
154 quantitative data and (ii) to determine if these patterns are specific to each pathosystem or show a
155 general trend. In addition, our work provides a new perspective and insight into appropriate genetic
156 and evolutionary models for representing quantitative plant-parasite interactions and for outcomes
157 for plant resistance management.

158

159 **Results**

160 We gathered 32 matrices corresponding to 15 plant-parasite pathosystems and containing
161 quantitative pathogenicity trait values (Table 1; Fig. 2). Among the 13 parasite species included, most
162 were fungi or oomycetes (five and four, respectively), while bacteria, nematodes, insects and viruses
163 were represented only once. Only three pathosystems included perennial (tree) plants and all plant
164 species were temperate-climate crops (or crops adapted to both temperate and tropical climates).
165 Each pathosystem included a set of strains belonging to the same parasite species and a set of
166 accessions belonging to the same plant species with four exceptions, matrices 9, 18, 19 and 26,
167 where accessions belonged to several closely-related plant species. Among the matrices, the number
168 of plant accessions varied from seven to 53 (median 12) and the number of parasite strains varied
169 from six to 98 (median 11.5). The number of matrix cells varied from 49 to 1470 (median 180). For
170 most pathosystems, we analyzed several matrices corresponding to either different pathogenicity
171 traits, different plant-parasite sets or different experiments. In order to meet the requirements of
172 methods that allow the estimation of nestedness and modularity of matrices, the pathogenicity traits
173 in each matrix were standardized into integer values ranging from 0 (minimal plant resistance and/or
174 maximal parasite pathogenicity) to 9 (maximal plant infection and/or minimal parasite
175 pathogenicity). We then tested for the occurrence of nestedness and modularity. For significance
176 assessment, the nestedness/modularity scores of the matrices derived from experimental data were
177 compared to those of simulated null-model matrices that are not expected to possess any nested or
178 modular pattern (Supplementary Methods 1). Nestedness (or modularity) is significant if the actual
179 matrix is more nested (or modular) than at least 95% of the matrices simulated under a given null
180 model (black numbers on grey background in Tables 2, 3 and 4). As there are many possible null
181 models and because their choice is crucial to conclude about the significance of nestedness or
182 modularity, we analyzed the performance of the different available nestedness/modularity
183 algorithms and of different null models by estimating their type I and type II error rates through a
184 simulation approach (Supplementary Methods 1; Tables S1 to S18).

185

186 *Ubiquitous nestedness in quantitative plant-parasite interactions*

187 First, we evaluated the performance of two algorithms, *WINE* and *wNODF* (Galeano et al. 2009;
188 Almeida-Neto and Ulrich 2011), to estimate the nestedness of the 32 matrices. Simulations revealed
189 that statistical significance with both null models C1 and R1 (or C2 and R2) provided the lowest false
190 positive rates for nestedness (Supplementary Methods 1; Tables S1 and S2). Under null models C1

191 and R1, matrices are generated column by column or row by row, respectively, and the cell numbers
192 are chosen randomly in order that (i) the marginal sums of cells and (ii) the numbers of zero-valued
193 cells are kept the same as in the actual matrix. To generate matrices under null models C2 and R2,
194 the cell values of the actual matrix are shuffled column by column or row by row, respectively.

195 With the *WINE* algorithm, nestedness values were quite high in general (from 0.46 to 1.04; mean
196 0.77 on a scale varying from 0 to ≈ 1). Thirty of the 32 matrices showed significant nestedness (p-
197 values ≤ 0.05) with null models C1, R1, C2 and R2 (Table 2). Only matrices 21 and 32 were not
198 significantly nested with either null model C1, R1, C2 or R2.

199 With the *wNODF* algorithm, nestedness estimates varied from 6.1 to 75.4 (mean 38.2) on a scale
200 varying from 0 to 100 and nestedness was significant for only 19 of the 32 matrices with null models
201 C1, R1, C2 and R2 (Table 2). This lower number of matrices showing nestedness is consistent with the
202 lower statistical power of *wNODF* compared to *WINE* (Supplementary Methods 1). As both methods
203 are based on different principles, the correlation of their nestedness scores among the 32 matrices is
204 only moderate (Pearson's $r = 0.37$; p-value = 0.038). Importantly, unlike the *WINE* method, *wNODF*
205 cannot estimate the nestedness of matrices devoid of zero-valued cells and underestimates
206 nestedness when zero-valued cells are scarce. Indeed, most of the matrices significantly nested with
207 *WINE* but not significantly nested with *wNODF* contained few zero-valued cells, most of which being
208 distributed on a single row or column. Consequently, the discrepancy between results obtained by
209 *WINE* and *wNODF* may be a bias due to the lack or peculiar distribution of the zero-valued cells. Five
210 more matrices (numbers 13, 15, 20, 29 and 31) were significantly nested with *wNODF* if 1-valued
211 cells or 1- and 2-valued cells were transformed into 0-valued cells.

212 With *wNODF* (but not with *WINE*), several matrices were less nested than at least 95% of the
213 matrices simulated under one or several null models (white numbers on black background in Table
214 2), a property that we will name anti-nestedness. Matrix 14 was significantly anti-nested with null
215 models N, C1, R1 and R2. For six other matrices, significant anti-nestedness was detected with one or
216 a few null models, a bias attributable to the small number of 0-valued cells (matrices 12, 23 and 24)
217 which disappeared largely when 1- and 2-valued cells were transformed into 0-valued cells.

218 Overall, taking into account the limitations of the *wNODF* algorithm, our analysis revealed that the
219 huge majority of the matrices (30/32; 94%) were significantly nested.

220

221 *Investigation of the biological significance of nestedness*

222 Adequacy of an additive linear regression model for pathogenicity matrices

223 The high and significant nestedness observed among most of the analysed matrices suggests that an
224 additive model combining pathogenicity QTLs in the parasites and resistance QTLs in the hosts, with
225 no QTL x QTL interactions between hosts and parasites, would fit well with the data (Fig. 1G). We
226 evaluated the performance of the linear regression model: ‘pathogenicity’ ~ ‘parasite strain’ + ‘plant
227 accession’, with no interaction term, on the datasets. For each plant accession-pathogen strain pair,
228 the mean pathogenicity value was considered for the ‘pathogenicity’ variable. The ‘parasite strain’
229 and ‘plant accession’ effects were highly significant (p-value < 0.0012), except for matrices 21 and 32
230 which were the only ones not significantly nested according to the *WINE* method (Table 2). Omitting
231 these two matrices, the multiple coefficient of determination (R^2) indicating model fit varied from
232 0.49 to 0.98 (mean 0.75) (Table 1), which lends support to the suggested genetic model. Moreover,
233 the multiple R^2 values of the linear regression model were significantly correlated with the
234 nestedness scores obtained with the *WINE* algorithm (Pearson’s $r = 0.73$; p-value = $2.6e-06$) across
235 the 32 matrices. They were only marginally correlated with the nestedness scores of the *wNODF*
236 algorithm ($r = 0.32$; p-value = 0.07).

237

238 Evaluating potential trade-offs: Host range breadth vs. pathogenicity in parasites and scope vs.
239 efficiency of resistance in host plants

240 The ubiquitous nestedness detected suggests a positive correlation between the host range breadth,
241 *i.e.* the percentage of host accessions that a parasite can efficiently infect, and the pathogenicity
242 level of the parasite. Similarly, a positive correlation is expected between the scope of the resistance
243 and the resistance efficiency of the plants. Given the continuous distribution of the quantitative
244 pathogenicity traits, we defined arbitrary pathogenicity thresholds to distinguish host and non-host
245 accessions for a given parasite strain, and to distinguish parasite strains included or not included in
246 the scope of the resistance of a given plant accession. Nine thresholds were defined, varying from
247 10% to 90% of the maximal pathogenicity value in the whole matrix by increments of 10%, and
248 allowed estimating the percentage of plant accessions included in the host range of each parasite
249 strain (*i.e.* the host range breadth) and the percentage of parasite strains included in the scope of
250 resistance of each plant accession. The mean Pearson’s coefficient of correlation (r) between host
251 range breadth and pathogenicity varied from 0.20 to 0.38 across the different threshold values
252 (mean 0.31). Depending on the threshold, from 23.1% (6/26 matrices) to 40.6% (13/32) (mean
253 31.9%) of the matrices showed significantly positive r values, whereas from 0 (0/11) to 9.7% (3/31)
254 (mean 4.8%) of the matrices showed significantly negative r values (Fig. 3). Note that the coefficient
255 of correlation could not be calculated for several matrices for some of the thresholds because of the

256 lack of pathogenicity values above (for correlation between host range breadth and pathogenicity) or
257 below (for correlation between resistance scope and efficiency) that threshold.

258 The mean r between resistance scope and efficiency varied from 0.18 to 0.59 across the different
259 threshold values (mean 0.39). Depending on the threshold, from 25.0% (6/24) to 46.9% (15/32)
260 (mean 35.8%) of the matrices showed significantly positive r values, whereas from 0 (0/32) to 9.4%
261 (3/32) (mean 2.9%) of the matrices showed significantly negative r values (Fig. 3).

262

263 *Rare cases of modularity in quantitative plant-parasite interactions*

264 We applied five algorithms to estimate the modularity of the 32 matrices (Newman and Girvan 2004;
265 Clauset et al. 2004; Newman 2006; Blondel et al. 2008; Traag and Bruggeman 2009; Supplementary
266 Methods 1). By maximizing a modularity score, these algorithms estimate the optimal number of
267 modules and the distribution of plant and parasite genotypes in the modules. Modularity scores
268 were low overall, with a maximum of 0.240 and a mean of 0.075, on a scale varying from 0 to 1
269 (Tables 3 and 4). The *fast greedy*, *louvain* and *leading eigenvector* methods provided highly similar
270 modularity scores among the 32 matrices, with Pearson's coefficients of correlation $r > 0.91$ (p -values
271 $\leq 1e-12$). Scores of the *edge betweenness* method were highly correlated with the previous three
272 methods ($0.58 < r < 0.74$; p -values $\leq 6e-04$) whereas scores of the *spinglass* method were moderately
273 correlated with the previous ones ($0.39 < r < 0.61$; p -values ≤ 0.027). Our analysis of the performance
274 of these methods showed that the *spinglass* algorithm had a very low rate of false positive
275 modularity, whatever the null model (Supplementary Methods 1). In contrast, the *fast greedy*,
276 *louvain* and *edge betweenness* algorithms had high rates of false positive modularity with several null
277 models, except models S (where cell values of the actual matrix are shuffled, with no constraints on
278 row or column marginal sums), C2 and R2 (Tables S7-S9).

279 According to the *spinglass* method, six matrices (numbers 5, 6, 10, 11, 14 and 17b) were significantly
280 modular with a majority of null models (Table 3), though their modularity scores were low (≤ 0.102).
281 Depending on the matrix, *spinglass* defined an optimal number of two or three modules, which
282 provided the maximal modularity score (Table 3; Fig. 4). In addition, matrices 8 and 22 were only
283 significantly modular with one null model. Evidence of modularity with the *edge betweenness*, *fast*
284 *greedy*, *louvain* and *leading eigenvector* methods was scarce, significant modularity being usually
285 observed for one of the null models S, C2 or R2 only and not for all methods (Table 4).

286 With all modularity methods, several matrices were less modular than at least 95% of the matrices
287 simulated under one or several null models (white on black numbers in Tables 3 and 4), a property

288 that we will name anti-modularity. For *spinglass*, only matrix 7 was significantly anti-modular with
289 null models N, C1 and R1 (Table 3). The other methods detected significant anti-modularity in most
290 matrices with most null models but suffered high rates of false positive anti-modularity for many null
291 models (Supplementary Methods 1; Tables S11-S13). Considering only matrices that are significantly
292 anti-modular with both null models C2 and R2, which correspond to the lowest rates of false
293 positives (null model CR2 in Tables S11 to S13), 13 matrices were significant with at least two
294 methods and three (matrices 17, 28 and 29) were significant with the four methods (Table 4). Results
295 obtained with the other matrices varied according to algorithms and null models, showing both
296 significant modularity and anti-modularity, which could be due to low type I error performances of
297 the algorithms for detection of modularity and/or anti-modularity.

298

299 *Investigation of the biological significance of modularity*

300 We examined the relevance of the detected modules for the six matrices showing significant
301 modularity with most null models with *spinglass* (Table 2) by analysing whether the plant and
302 parasite genotypes belonging to each module shared common properties (common resistance gene
303 or QTL for plants; common pathogenicity factor for parasites; common origin for plants or parasites).

304 For matrix 5 (*Puccinia hordei*-barley), two modules were detected (Fig. 4). The first one grouped the
305 five accessions with resistance QTLs *Rphq3* and *Rphq11*, showing delayed infection with most isolates
306 of the second module, and one accession carrying QTLs *Rphq1*, *Rphq2* and *Rphq3*, showing delayed
307 infection with almost all isolates (González et al. 2012). The second module contained four
308 accessions with either no resistance QTL or QTL *Rphq18*, that were quickly infected by almost all
309 isolates. The country of origin or date of collection of the isolates did not explain their distribution in
310 the two modules (Marcel et al., 2008).

311 For matrix 6 (*Venturia inaequalis*-apple), three modules were detected. The first one grouped the
312 eight accessions carrying QTL *T1* and the four *V. inaequalis* isolates collected on apple trees carrying
313 *T1* (Laloi et al. 2017). The two other modules grouped (i) the remaining accessions that were either
314 carrying no resistance QTL or QTLs F11 or F17 that have only a low effect on disease reduction and
315 (ii) isolates collected on these accessions. One of these modules grouped a single isolate and a single
316 accession. Infections were on average high within all modules and low between any pair of modules.

317 Two modules were also detected for matrix 14 (*Zymoseptoria tritici*-bread wheat). These modules
318 could be partially explained by the interaction between the resistance gene *Stb6* (Saintenac et al.
319 2018), that confers a high level of resistance in the absence of a hypersensitive response, and the

320 pathogen avirulence gene *AvrStb6* (Zhong et al. 2017). Six of the eight cultivars in the first module
321 carry *Stb6*, while at least six of the seven cultivars in the second module do not carry *Stb6*. Moreover,
322 the 44 fungal isolates structuring the first module are pathogenic on *Stb6* while the 54 isolates from
323 the second module are either pathogenic or not pathogenic on *Stb6*.

324 Concerning matrices 10, 11 (*Podosphaera xanthii*-melon) and 17b (*Phytophthora capsici*-pepper),
325 three modules were detected but there was no evidence of similarity in the genetic composition of
326 accessions, the presence of particular resistance genes or QTLs or the origin of isolates belonging to a
327 same module.

328

329 *Modularity of reverse matrices*

330 To test the occurrence of IMA patterns (Fig. 1F), we also analyzed the modularity of the 32 matrices
331 transformed such that a grade of 0 corresponds to the maximal plant susceptibility and grades 1 to 9
332 correspond to the range of increasing plant resistance (hereafter “reverse matrices”). Using the
333 *spinglass* algorithm, four matrices (numbers 10, 11, 14 and 15) showed significant but low modularity
334 (≤ 0.078) with either null models C1 and R1 or C2 and R2. Depending on the matrix, *spinglass* defined
335 an optimal number of two to five modules (Fig. 5).

336 The modules identified in reverse matrices 14 and 15 using the *spinglass* algorithm were biologically
337 more meaningful than the two modules previously identified for matrix 14. Matrices 14 and 15
338 correspond to two different phenotypic traits measured in the same plant-parasite interactions (i.e.
339 necrosis and sporulation, respectively). Interestingly, modules identified in the two matrices were
340 similar but not identical since five modules were identified in matrix 14 and four modules were
341 identified in matrix 15. This may reflect differences in the genetic determinism of the two phenotypic
342 traits measured or differences in the mechanisms of various *Stb* resistance genes. For matrix 14,
343 three modules correspond to the presence of resistance genes *Stb7* (one cultivar), *Stb9* (three
344 cultivars) and *Stb6* (four cultivars), one module to cultivars carrying various *Stb* genes (three
345 cultivars), and one module to susceptible (or partially resistant) cultivars (four cultivars). For matrix
346 15, the modules corresponding to the presence of *Stb6* and *Stb9* are also identified (with an
347 additional cultivar in the *Stb6* module), the module corresponding to susceptible cultivars as well
348 (with two additional cultivars), and the cultivar Salamouni carrying *Stb13* and *Stb14* forms the fourth
349 module. As above, there was no evidence of similarity in the composition of accessions and isolates
350 belonging to the same module for reverse matrices 10 and 11.

351 Overall, considering both the initial and reverse matrices, our analysis revealed that only a minority
352 of the matrices (7/32; 22%) were significantly modular.

353

354 **Discussion**

355 There is nothing more fundamental to the concepts in Plant Pathology as a science and to the
356 practical strategies used for managing plant health than the host range of a parasite and the scope of
357 resistance of a plant (Morris and Moury 2019). Based on the patterns in matrices of plant-parasite
358 interactions, we can conceive and test hypotheses about the molecular and evolutionary processes
359 that underlie plant-parasite interactions, develop robust diagnostic tools, design breeding programs
360 and strategies for deploying resistant cultivars, and construct models to anticipate disease
361 emergence. Given the complexity of the mechanisms involved in disease, it would be reasonable to
362 assume that the particularities of each pathosystem would be an impediment to identifying universal
363 principles that can guide these efforts. However, here we have used network-based analyses to
364 reveal the quasi-universal principle that the structure of quantitative matrices of plant-parasite
365 interactions is nested. Indeed, evidence of nestedness was found in 94% (30/32) of the matrices that
366 we analyzed and one of the two non-nested matrices (number 32) was one of the smallest ones,
367 which may have precluded the detection of a significantly nested pattern. Our results were based on
368 statistically robust analyses of quantitative assessments of compatible interactions between hosts
369 and parasites for large interaction matrices involving from 49 to 1470 (median 180) host-parasite
370 combinations. Quantitative data are key to the accuracy and genericity of these analytical methods.
371 Indeed, in a study of 52 published matrices containing data on plant-pollinator, plant-seed disperser
372 and parasitoid-host interactions, Staniczenko et al. (2013) found evidence of nestedness in only 3%
373 of matrices including quantitative data, whereas the same matrices considered in a binary manner
374 showed evidence of nestedness in 98% of cases.

375 Network theory has its origins in the study of social networks and in ecology of interacting organisms
376 (Patterson and Atmar 1986). Ecological networks are typically identified by counting *in natura* the
377 interactions between (or co-occurrence of) two sets of taxa. Evidence of nestedness was frequent for
378 all kinds of matrices, including interactions between hosts and symbionts, either mutualistic or
379 parasitic (Bascompte et al. 2003; Joppa et al. 2010; Dormann et al. 2017). A number of factors that
380 are external to the interacting organisms can affect properties of such ecological networks. For
381 example, nestedness increases with the abundance of taxa (Joppa et al. 2010; Staniczenko et al.
382 2013; Suweis et al. 2013; Valverde et al. 2018), with heterogeneous distribution of connections, *i.e.*
383 of numbers of links between interacting taxa (Jonhson et al. 2013), with the occurrence of broad

384 connectivities (Feng and Takemoto 2014) and with spatially-limited interactions between taxa
385 (Valverde et al. 2017). These analytical methods were recently used to analyse host-symbiont
386 interactions resulting from cross-inoculation experiments, where every host taxon was inoculated
387 with every symbiont taxon, and the compatibility of each host-symbiont pair was reported in the
388 matrix (Flores et al. 2011; Flores et al. 2013; Weitz et al. 2013). The structural patterns of such
389 matrices, where all host-symbiont pairs are evaluated under the same experimental and
390 environmental conditions, are mainly the result of intrinsic, mostly genetic, differences between host
391 or symbiont taxa.

392 Network analyses can also be strongly affected by the choice of null models (Gotelli and Graves
393 1996). This is why we conducted a thorough evaluation of the performance of several null models
394 with simulations (Supplementary Methods 1). The null models should keep, as much as possible,
395 everything identical to the actual matrix apart from the pattern of interest, nestedness or
396 modularity. Many null models have unacceptably loose constraints. For example, null models that do
397 not force row or column marginal sums to be constant create distributions of taxa that do not match
398 those usually observed, leading to falsely positive nestedness (Brualdi and Sanderson 1999; Joppa et
399 al. 2010). Accordingly, high rates of false positives were observed with null models N and S in our
400 simulations (Tables S1 and S2). Since parasites typically differ greatly in the number of hosts they
401 exploit and the efficiency with which they exploit them, we did not want null models to detect
402 significant nestedness when the heterogeneity of infection was shuffled randomly among hosts, as
403 was frequently observed for null models N and S with test matrices M1R to M5R (Tables S1 and S2).
404 Null models R1 and R2 that force row marginal sums to be constant avoided this problem (Tables S1
405 and S2). The same was true for the scope and efficiency of resistance that differ greatly between
406 plant accessions. In that case, the C1 and C2 null models efficiently avoided an excess of falsely
407 positive nestedness due to the heterogeneity of resistance (because C1 and C2 are equivalent to R1
408 and R2 when the rows and columns of the matrix are exchanged, which leaves the nestedness scores
409 unchanged; data not shown). Overall, to account for both plant resistance and parasite infection
410 heterogeneities, we found that the CR1 (or CR2) null model, that combines null models C1 and R1 (or
411 C2 and R2, respectively), is the most efficient as it showed acceptable type I error rates
412 (Supplementary Methods 1). Null model B, based on Patefield's (1981) algorithm, maintains both the
413 row and column marginal sums of the actual matrix. However, it does not maintain the connectance
414 (*i.e.* number of non-zero-valued cells of the matrix), which has a strong impact on the estimation of
415 nestedness. Consequently, the type I error rates associated with null model B were frequently higher
416 than those obtained with models CR1 or CR2. Moreover, using quantitative instead of binary data

417 contributed to lowering the nestedness false positive rate (Staniczenko et al. 2013; Dormann et al.
418 2017).

419 Overall, we obtained strong and consistent evidence of nestedness for almost all matrices (except
420 matrices 21 and 32), whatever the parasite type, the plant species or the pathogenicity trait
421 measured. Nestedness was linked to two important features of quantitative plant-parasite matrices:
422 (i) scarcity and/or low level of statistical interactions between plant and parasite genotypes in terms
423 of infection intensity and (ii) lack of trade-offs between host range and pathogenicity among parasite
424 strains and between efficiency and scope of the resistance among plant accessions.

425 The former feature is supported by the fact that an additive linear model - containing only a plant
426 accession effect and a parasite strain effect with no interaction term - showed high multiple
427 coefficients of determination (from 0.49 to 0.98) across matrices (Table 1). This result is compatible
428 with a genetic model where pathogenicity in the parasite and resistance in the host plant are
429 determined by a varying number of QTLs, but the statistical interaction between effects of QTLs from
430 the parasite and QTLs from the host is rare and/or of small magnitude (Table 1; Fig. 1G). In other
431 words, plants and parasites differ by their QTL assemblage (i.e. QTL numbers and/or effects) but
432 plant resistance QTLs have similar effects towards all parasite strains and, reciprocally, parasite
433 pathogenicity QTLs have similar effects towards all plant genotypes. Quantitative models usually
434 used to analyse empirical data on plant-parasite interactions are quite simplistic, *e.g.* assuming or not
435 a statistical interaction between plant and parasite genotypes (Parlevliet 1977). Models that are
436 more complex have been proposed in the frame of theoretical modelling (*e.g.* Fenton et al. 2009) but
437 their relevance to represent biological data was not evaluated. Importantly, we do not argue that
438 evidence of nestedness supports a single genetic model of plant-parasite interaction. Instead, we
439 suggest that an additive linear model with a plant accession and a parasite strain effects is the
440 simplest model that accounts for the empirical data but we cannot exclude that other models could
441 be suitable, like the modified GFG model of Fenton *et al.* (2009). A future challenge, requiring more
442 in-depth genetic studies, would be to evaluate the adequacy of these different models to represent
443 empirical plant-parasite interactions. New analytical methods can provide a better understanding
444 and quantification of host-parasite genetic interactions, such as the host-parasite joint genome-wide
445 association analysis recently developed by Wang et al. (2018). Applied to the *Arabidopsis thaliana*-
446 *Xanthomonas arboricola* pathosystem, this model showed that 44%, 2% and 5% of the phenotypic
447 variance could be explained respectively by the parasite strain, the host accession and the parasite-
448 host interaction. As in our results, only a small parasite-host interaction effect was detected.

449 The latter feature of quantitative plant-parasite matrices is supported by the fact that we observed a
450 majority of positive, rather than negative correlations (i.e. trade-offs), between the infectivity and
451 the breadth of host range of parasites on the one hand and, especially, between the efficiency and
452 scope of the resistance of plants on the other hand (Fig. 3). Few studies have examined the
453 relationships between the scope and efficiency of plant resistance. In contrast with our results,
454 Barrett et al. (2015) hypothesized evolutionary trade-offs between resistance efficiency and scope
455 because quantitative resistance had a broader scope compared to qualitative resistance in the *Linum*
456 *marginale* – *Melampsora lini* interactions. The difference between our studies could be that we
457 focussed on quantitative resistance and included few qualitative resistance genes in our dataset (or
458 these were overcome by most parasite strains). The positive correlation between parasite infectivity
459 and host range breadth contrasts with qualitative host-parasite interactions and especially the GFG
460 model, where the expansion of the host range of parasites is associated with a cost in fitness during
461 infection of the previous hosts. Such so-called “virulence costs” have been experimentally measured
462 in many plant-parasite systems, including viruses (Jenner et al. 2002; Desbiez et al. 2003; Janzac et al.
463 2010; Poulicard et al. 2010; Fraile et al. 2011; Ishibashi et al. 2012; Khatabi et al. 2013), fungi (Bahri
464 et al. 2009; Huang et al. 2010; Caffier et al. 2010; Bruns et al. 2014), oomycetes (Montarry et al.
465 2010), bacteria (Vera Cruz et al. 2000; Leach et al. 2001; Wichmann and Bergelson 2004) or
466 nematodes (Castagnone-Sereno et al. 2007), and could explain why universal pathogenicity is not
467 fixed in pathogen populations (Tellier and Brown 2011). For quantitative plant resistance, few studies
468 have estimated the occurrence of pathogenicity costs. Montarry et al. (2012) showed a cost for PVY
469 to adapt to a quantitative pepper resistance when inoculated to a susceptible pepper genotype,
470 whereas Delmas et al. (2016) showed, on the opposite, that there was no fitness cost associated with
471 the adaptation of *Plasmopara viticola* to partially resistant grapevine varieties. Fournet et al. (2016)
472 even highlighted that nematode populations that had adapted to potato quantitative resistance were
473 more pathogenic on a susceptible potato genotype than were naïve nematode populations. The
474 present study focused mostly on interactions between plants and parasites at the intraspecific level,
475 but other studies have revealed a similar trend when strains of a given parasite species are
476 confronted with numerous plant species. For example, a positive correlation was observed between
477 species host range and pathogenicity for *Pseudomonas syringae* (Morris et al. 2000, 2019). For this
478 bacterium, the most pathogenic strains were also the most ubiquitous in the environment,
479 suggesting also an absence of trade-off between host range and dispersal capability or survival in the
480 environment (Morris et al. 2010).

481 In contrast to nestedness, we obtained little evidence of modularity among the matrices that we
482 analysed. Modularity scores were low for all matrices. In only seven matrices, representing either

483 infection or resistance scores (i.e. reverse matrices), did we detect significant modularity with a
484 majority of null models (Tables 3 and 4; Fig. 4 and 5). For four of these matrices (matrices 5, 6, 14 and
485 15), modularity was linked to the presence of particular resistance genes or QTLs in the plant
486 accessions and, for the parasite strains, to the presence of particular avirulence genes or to a
487 common origin in terms of host genotype. For the remaining matrices (10, 11 and 17b), no common
488 property could be found for plant accessions and parasite strains belonging to the same module. The
489 lack of modularity of infection matrices and of reverse matrices suggests that the MA and IMA
490 genetic models are either inadequate to represent the structure of quantitative plant-parasite
491 interactions or explain only marginally their structure (Fig. 1E,F).

492

493 **Conclusion**

494 The ubiquitous nested patterns observed in quantitative plant-parasite interaction matrices have
495 important implications for our understanding and management of plant diseases. They can help infer
496 the underlying genetic bases of quantitative aspects of disease manifestation and their evolution.
497 Our results are compatible with an additive model comprising a plant resistance effect, a parasite
498 pathogenicity effect and no (or little) plant-parasite interaction effect.

499 A major enigma that we highlight is the apparent lack of trade-off between pathogenicity and host
500 range breadth among strains of a parasite, which has important implications on the efficiency of
501 plant resistance management through cultivar rotation, mixtures or mosaics. Indeed, these strategies
502 rely at least in part on a counter-selection of the most pathogenic parasite strains by a diversification
503 of plant cultivars (Brown 2015). The efficiency of these strategies would certainly be reduced in
504 absence of costs of adaptation to plant resistance. Therefore, in absence of such costs, the efficiency
505 of the rotation, mixtures or mosaic strategies would rather depend on barrier effects designed to
506 limit parasite dispersal in agricultural landscapes.

507

508 **Materials and Methods**

509 *Datasets*

510 To be able to analyse plant-parasite interaction networks, we selected datasets containing at least 6
511 plant accessions and 6 parasite strains. A brief description of these datasets is provided in Table 1
512 and in the following text.

513

514 Matrices 1 to 4: *Pseudomonas syringae*-*Prunus armeniaca* (apricot)

515 Nine strains of *Pseudomonas syringae*, the causal agent of bacterial canker of apricot, were
516 inoculated on dormant tissues of twenty apricot cultivars chosen according to their differential
517 susceptibility in orchard conditions. The strains were chosen mainly within phylogroups 1 and 2, the
518 most abundant groups of *P. syringae* in contaminated apricot orchards in France (Parisi *et al.* 2019).
519 Seven strains were isolated from symptomatic trees and two in crop debris and soil. Bacterial
520 inoculum was prepared by cultivation on King's B medium for 48h at 24°C. The concentration of the
521 bacterial suspension was adjusted at 10⁸ CFU.ml⁻¹. A volume of 25 µl of inoculum was deposited at
522 the level of a wound made superficially with a scalpel on the bark of one-year-old twigs grown in
523 orchard. Five months after inoculation, twigs were removed and the length of flat zone around the
524 inoculation point at the surface of the shoot (matrices 1 and 2) and the length of browning zone
525 around the inoculation point below the bark of the shoot (matrices 3 and 4) were measured. Two
526 independent tests were performed in 2017 (matrices 1 and 3) and 2018 (matrices 2 and 4).

527

528 Matrix 5: *Puccinia hordei*-*Hordeum vulgare* (barley)

529 Fourteen *Puccinia hordei* isolates (from Europe, Morocco, Israel and the USA) were inoculated on a
530 differential series of 12 *H. vulgare* lines carrying different *Rphq* QTLs (González *et al.* 2012). The first
531 seedling leaves of each barley line were inoculated with ≈240 spores/cm². The relative latency period
532 (RLP) (Table 3 in González *et al.* 2012) was estimated by the number of hours from inoculation to the
533 moment at which 50% of the ultimate number of uredinia was visible.

534

535 Matrices 6 to 8: *Venturia inaequalis*-*Malus domestica* (apple tree)

536 Grafted plants of different apple accessions (*Malus domestica*) carrying resistance QTLs (*T1*, *F11*, *F17*,
537 *F11 + F17* or *T1 + F11 + F17*) or no resistance QTL were inoculated in controlled conditions with isolates
538 of *Venturia inaequalis*, a fungal pathogen responsible of apple scab. The percentage of sporulating
539 leaf area was assessed from 8 to 21 days post inoculation (dpi) on a scale with eight levels: 0 = no
540 visible symptom, 0.5 = 0–1%, 3 = 1–5%, 7.5 = 5–10%, 17.5 = 10–25%, 37.5 = 25–50%, 62.5 = 50–75%,
541 and 87.5 = 75–100%.

542 Matrix 6 (Laloi *et al.* 2017) consisted of interactions between 10 *V. inaequalis* isolates sampled in one
543 orchard (Angers, France) on apple trees carrying *T1*, *F11+F17*, *T1+F11+F17* or no QTL and 14 apple
544 accessions carrying the matching resistance QTL or no QTL.

545 Matrix 7 (Caffier et al. 2016) consisted of interactions between 14 *V. inaequalis* isolates sampled in one
546 orchard (Angers, France) on apple trees carrying or not *T1* and 12 apple accessions carrying or not *T1*
547 (with six accessions for each of the two classes). Matrices 6 and 7 represent the Area Under the Disease
548 Progress Curve (AUDPC) of the percentage of sporulating leaf area from eight to 21 dpi.

549 Matrix 8 (Caffier et al. 2014) consisted of interactions between 24 *V. inaequalis* isolates sampled in
550 two orchards (Lanxade and Villeneuve d'Ascq, France) on apple trees carrying *F11*, *F17*, *F11+F17* or
551 no QTL and eight apple accessions carrying the matching QTL or no QTL (with two accessions for each
552 of the four classes). Matrix 8 represents the percentage of sporulating leaf area 14 dpi.

553

554 Matrix 9: *Botrytis cinerea*-*Solanum lycopersicum* / *Solanum pimpinellifolium* (tomato)

555 Leaves of 12 tomato accessions (six domesticated accessions of *Solanum lycopersicum* and six
556 accessions of the close wild relative *S. pimpinellifolium*) were infected with single droplets of spore
557 suspensions of 94 *B. cinerea* isolates. The size of lesions was measured from digital images 72 hours
558 after inoculation (Soltis et al. 2019). One isolate was poorly infectious on all tomato accessions (grade
559 0 after data transformation) and was withdrawn.

560

561 Matrices 10 and 11: *Podosphaera xanthii*-*Cucumis melo* (melon)

562 Nineteen melon differential lines were inoculated with 26 *Podosphaera xanthii* isolates collected in
563 2013 and 2014 in melon, squash, watermelon and cucumber crops in Southern Europe or Northern
564 Africa (France, Spain, Italy, Morocco, Turkey, Greece). Each *P. xanthii* isolate was propagated on
565 cotyledons of *Lagenaria ciceraria* for seven days and spores were blown on eight leaf disks per melon
566 line-*P. xanthii* isolate combination using an inoculation tower (Perchepped et al. 2005). Sporulation
567 intensity was scored 14 days after inoculation and data were transformed in percentage of leaf disk
568 surface using the class mean as suggested by Nicot et al. (2002): 0 = 0%, 1 = 2.5%, 2 = 7.5%, 3 =
569 17.5%, 4 = 37.5%, 5 = 67.5%, 6 = 82.5%, 7 = 92.5%, 8 = 97.5%, and 9 = 100%. The mean score for
570 melon accession - *P. xanthii* isolate combinations was reported in matrix 10. For matrix 11, 31
571 isolates were inoculated to 19 differential lines on leaves of entire plants. The sporulation intensity
572 was scored similarly as for leaf disks using a 0 to 9 scale. The mean score for melon accession - *P.*
573 *xanthii* isolate combinations was reported in matrix 11.

574

575 Matrices 12 to 15: *Zymoseptoria tritici*-*Triticum aestivum* (bread wheat) or *T. turgidum* subsp. *durum*
576 (durum wheat)

577 Matrices 12 and 13 were built by inoculating 12 lineages from a durum wheat landrace called
578 Mahmoudi with 15 *Zymoseptoria tritici* isolates. The 12 plant lineages were fixed from individuals
579 coming from a single field at Joumine in Tunisia and corresponded to 12 different multilocus genotypes
580 (MLGs) as defined previously by Ben Krifa et al. (2020). The 15 isolates were collected *in situ* either
581 from the landrace Mahmoudi or from the cultivar Karim, at Joumine in 2018. Matrices 14 and 15 were
582 built by inoculating 15 bread wheat cultivars (*Triticum aestivum*), 12 of which carrying different *Stb*
583 resistance genes, with 98 *Z. tritici* isolates collected mostly on cultivars Apache and Premio, all over
584 France between 2009 and 2010. These bread wheat cultivars belong to a series of differential
585 genotypes used to characterize the pathogenicity of *Z. tritici* isolates. All wheat-*Z. tritici* pairwise
586 confrontations were evaluated under controlled conditions, in growth chambers at 18°C/22°C
587 night/day and 16 hours light at 300 $\mu\text{mol}\cdot\text{m}^{-2}\cdot\text{s}^{-1}$. The first true leaf of 16-day-old seedlings were marked
588 with a black felt to delimit a 7.5 cm length that was inoculated with a solution of water containing 10^6
589 spores.mL⁻¹ and one drop of Tween®20 per 15 mL. The inoculum was applied with a square-tipped flat
590 paintbrush six times on each leaf, repeated twice. After inoculation the plants were placed in
591 transparent polyethylene bags for 72 hours to initiate infection. At 10 dpi, *i.e.* before the appearance
592 of symptoms, leaves above the inoculated leaf were cut to homogenize light exposure. Visual
593 estimations of necrotic leaf area and sporulating leaf area were done at 14 dpi, 20 dpi and 26 dpi for
594 matrices 12 and 13, and only once at 21 dpi for matrices 14 and 15. For matrices 12 and 13, these
595 observations were used to calculate, for each plant lineage-isolate combination, an area under disease
596 progress curve (AUDPC) for the percentages of necrotic and sporulating leaf areas. The interactions for
597 matrices 12 and 13 were evaluated on three leaves repeated twice in time (total of six leaves) and for
598 matrices 14 and 15 on three leaves repeated thrice in time (total of nine leaves).

599

600 Matrices 16, 17 and 17b: *Phytophthora capsici*-*Capsicum annuum* (pepper)

601 To build matrix 16, the pathogenicity of six isolates of *Phytophthora capsici*, the causal agent of root
602 and crown rot of chilli and bell peppers, collected in pepper fields in Algeria was measured in ten
603 *Capsicum annuum* cultivars (F₁ hybrids or inbred lines) (Messaouda et al. 2015). Six plants per accession
604 were inoculated by depositing a plug of 4 mm in diameter of mycelium of *P. capsici* cultivated on V8
605 medium on the fresh section of the primary stem extemporaneously decapitated (Lefebvre and Palloix
606 1996). Inoculated plants were kept in a growth chamber under controlled conditions with 12h
607 photoperiod, a temperature of 22 ± 2°C and 100% relative humidity. *P. capsici* progresses to the

608 bottom of the stem causing a necrosis of the stem. The length of stem necrosis at 15 dpi is reported in
609 matrix 16.

610 For matrix 17, 53 accessions of *C. annuum* were inoculated by six isolates of *P. capsici*. The *C. annuum*
611 accessions originated from 20 countries from America, Europe, Asia and Africa, and included
612 accessions that had different levels of partial resistance to isolate *P. capsici* 'Pc101' and a few
613 susceptible accessions. The six *P. capsici* isolates were isolated from pepper plants in France and
614 Turkey, were of A1 mating type and differed in pathogenicity. A minimum of six plants per accession,
615 seven-eight week old, were inoculated as described for matrix 16. Inoculated plants were kept in a
616 growth chamber under controlled conditions with a photoperiod of 12h at 24°C under artificial light
617 and 22°C at obscurity. The length of stem necrosis was measured six times from three to 21 dpi and
618 the Area Under the Disease Progress Curve (AUDPC) of necrosis length was considered in matrix 17.
619 Because matrix 17 contained a large number of zero-values cells, matrix 17b was derived by
620 withdrawing redundant columns and columns entirely made of zero-valued cells.

621

622 Matrix 18: *Phytophthora infestans*-*Solanum lycopersicum*

623 Matrix 18 was built by inoculating eight *Solanum* sp. accessions with seven isolates of *Phytophthora*
624 *infestans*, the causal agent of tomato late blight. The accessions consisted of three inbred lines of
625 cultivated tomato (*Solanum lycopersicum*) and five accessions of the wild relative species *S.*
626 *pimpinellifolium*, *S. habrochaites* and *S. pennellii*. Some of them are known to carry the *Ph-1*, *Ph-2* or
627 *Ph-3* genes, controlling resistance to races 0, 1 and 2 of *P. infestans*, respectively. The *P. infestans*
628 isolates were collected on tomato or potato plants in France and Poland and were chosen because
629 they varied in mating type (A1 or A2) and differed in pathogenicity. Mycelium was grown on pea juice-
630 based agar medium for 10 days and six plants per accession, 3-4 week old, were inoculated using the
631 protocol described for matrix 16 (Danan et al. 2009). Inoculated plants were kept in a growth chamber
632 under controlled conditions with a photoperiod of 14h at 21°C under artificial light and 17°C at
633 obscurity. High humidity was maintained by artificial mist. Stem necrosis length was scored four times
634 from three to 14 dpi and the AUDPC was calculated.

635

636 Matrix 19: *Aphanomyces euteiches*-Fabaceae (pea, vetch, faba bean, alfalfa)

637 Eight accessions from four leguminous species (pea, alfalfa, vetch, faba bean), which previously
638 showed various levels of resistance, were inoculated with 34 *Aphanomyces euteiches* isolates
639 sampled from the main French pea growing regions in a growth chamber (thermo period: 25/23°C
640 and 16h photoperiod). Seven-day-old plants (5 plants * 4 replicates * 2 experiments for each
641 accession-isolate combination) were inoculated by applying 5 mL of a zoospore suspension adjusted

642 to 5.10^3 spores / mL. After inoculation, the vermiculite substrate was saturated with water to provide
643 favorable conditions for infection. After 10 days, the plants were carefully removed from the
644 vermiculite, the roots were washed in tap water and disease severity (DS) was scored on each plant
645 using a 0–5 scale: 0 = no symptoms; 1 = traces of discoloration on the roots (<25%); 2 = discoloration
646 of 25 to 50% of the roots; 3 = discoloration of 50 to 75% of the roots; 4 = discoloration of >75% of the
647 roots; 5 = dead plant. ANOVA was performed with the DS score as the dependent variable, the *A.*
648 *euteiches* isolate and the plant accession as fixed factors and the replicate and experiment as random
649 factors. From the ANOVA, least square means (LSmeans) were calculated for each *A. euteiches*
650 isolate-plant accession combination. In the present study, LSmeans values of root DS scores were
651 analysed. More details are provided in Quillévéré-Hamard et al. (2018).

652

653 Matrix 20: *Aphanomyces euteiches*-*Pisum sativum*

654 Ten pea accessions were inoculated with 43 *A. euteiches* isolates sampled from the main French pea
655 growing regions in a growth chamber. The ten pea accessions consisted of (i) eight Near-Isogenic-
656 Lines (NILs) carrying one, two, three or five resistance alleles at main QTLs, in a common genetic
657 background and (ii) two control lines, including one susceptible variety and one highly resistant line.
658 The experimental design, inoculation procedure, disease scoring scale and statistical analysis were
659 similar to that described for matrix 19, except for inoculum concentration (2.10^2 spores / mL) and the
660 scoring date (seven days after inoculation). LSMeans values of root DS scores were used. More details
661 are provided in Quillévéré-Hamard et al. (2020).

662

663 Matrices 21 and 22: *Plasmopara viticola*-*Vitis vinifera* (grapevine)

664 A set of 33 *Plasmopara viticola* strains, the causal oomycete of grapevine downy mildew, was
665 inoculated on eight grapevine varieties. The host panel was constituted of seven grapevine varieties
666 carrying the main resistance factors currently used in European breeding programs (*Rpv1*, *Rpv3.1*,
667 *Rpv3.2*, *Rpv5*, *Rpv6*, *Rpv10* and *Rpv12*) and one susceptible variety (Chardonnay). Cuttings from these
668 varieties were grown in a glasshouse under natural photoperiod. Each strain-variety combination was
669 replicated on five leaf discs from five different plants that were excised in the fourth leaf below the
670 apex. Leaf discs were sprayed with 4 mL of a suspension of 10^5 / mL sporangia of *P. viticola*. They
671 were incubated in a climatic chamber for six days at 18°C with 12h/12h light/dark photoperiod. At six
672 dpi, necrosis was rated on a scale of 0 to 4, based on the number of necroses counted per leaf disk (0
673 = no necrosis; 1 = <10 necroses; 2= from 10 to 30 necroses; 3= from 30 to 60 necroses; 4= > 60

674 necroses) (matrix 21) and sporulation was assessed on leaf discs by automatic image analysis
675 (number of black pixels on the total leaf disc area) (matrix 22).

676

677 Matrices 23 and 24: *Aphis gossypii*-*Cucumis melo*

678 Matrices 23 and 24 were obtained through assessment of the resistance of 13 melon accessions to
679 nine aphid (*Aphis gossypii*) clones (Boissot et al. 2016). The host panel consisted in twelve partially-
680 resistant lines originating from Africa, India, China, Asia and Far East Asia, Mediterranean basin and
681 North America and a susceptible cultivar originating from Mediterranean basin. Two lines were wild
682 accessions and the others from breeding programs. They contained at least one to three homologs of
683 *Vat*, a gene conferring resistance to *A. gossypii*. The 13 melon lines belonged to three genetic groups
684 representative of melon diversity (Boissot et al., submitted). The aphid panel consisted in nine clones
685 collected in France and French West Indies. Except clone NM1 that was observed on plant species
686 belonging to six families, the clones have been observed exclusively (or almost exclusively) on
687 cucurbit plants and belong to the same genetic cluster.

688 For phenotyping, ten adult aphids were deposited on melon plantlets. Three days later, the number
689 of aphids remaining on the plantlets was recorded as the 'Acceptance' parameter (matrix 23). Seven
690 days after aphid deposition, the adults were counted, and the density of nymphs was estimated on a
691 scale of 0 to 6. The 'Colonization' parameter was calculated as [density of nymphs + ln(number of
692 adults + 0.001)] (matrix 24). The 'Acceptance' and 'Colonization' parameters were collected for at
693 least eight plantlets of each melon accession. Each test was conducted with one aphid clone on a
694 subset of melon accessions.

695

696 Matrices 25 and 26: *Globodera pallida*-*Solanum tuberosum* (potato)

697 Matrix 25 was obtained through the inoculation of 20 populations of the potato cyst nematode
698 *Globodera pallida* on ten potato accessions. Those potato accessions were characterized by different
699 levels of quantitative resistance. A susceptible potato cultivar, Désirée, was also used as a control.
700 Among the 20 *G. pallida* populations, 14 came from South-America (Peru and Chile) and six from
701 Europe. To perform *G. pallida* inoculation, ten cysts were locked in a tulle bag and placed in a pot
702 three-quarter filled with a soil mixture free of cysts (2/3 sand and 1/3 natural field soil). Four
703 replicates were performed for each potato accession - *G. pallida* population combination, *i.e.* for
704 each *G. pallida* population, four bags were inoculated to four tubers of the same potato accession.
705 One potato tuber was planted per pot and covered with the same soil mixture. Potato plants grew in

706 the greenhouse, under controlled conditions (15°C night during 8h and 20°C day during 16h), for 120
707 days. After 120 days, newly formed cysts were extracted from the soil, using a Kort elutriator. The
708 number of newly formed cysts was counted using a magnifying stereomicroscope, and divided by the
709 number of newly formed cysts produced on the susceptible cultivar Désirée (relative value).

710 For matrix 26, the measured fitness trait was the hatching of cysts which is induced by host root
711 exudates. It was produced using a cross-hatching assay between 13 populations of *G. pallida* and
712 root exudates from 12 wild potato accessions, belonging to species *Solanum huancabambense*, *S.*
713 *mochiquense*, *S. sogarandinum*, *S. ambosinum*, *S. medians*, *S. pampasense*, *S. santalallae*, *S.*
714 *marinasense*, *S. sparsipilum*, *S. raphanifolium*, *S. limbaniense* and *S. leptophyes*, to test the
715 hypothesis of local adaptation between Peruvian *G. pallida* populations and Peruvian wild potato
716 accessions (Gautier et al. 2020). All details about *G. pallida* populations, root-exudates and the *in*
717 *vitro* hatching assay are available in Gautier et al. (2020). Briefly, three cysts of each population were
718 put on a sieve in 1.5 mL of root exudates (with four to five replicates) and after 30 days, the number
719 of hatched juveniles was counted. At the end of the experiment, cysts were crushed and the number
720 of unhatched viable eggs was counted, in order to calculate a hatching percentage.

721

722 Matrices 27 to 32: *Potato virus Y-Capsicum annum*

723 The *Capsicum annum* accessions were doubled-haploid lines issued from the F₁ hybrid between
724 accessions Perennial, carrying several *Potato virus Y* (PVY) resistance QTLs, and the susceptible
725 accession Yolo Wonder. They were chosen based on the lack of a major-effect resistance gene but
726 contrasted levels of quantitative resistance (Caranta et al. 1997). The PVY populations were issued
727 from cDNA clones of isolates SON41p and LYE84.2 and recombinants between these two cDNA
728 clones (Montarry et al. 2012). *Capsicum annum* accessions were mechanically inoculated with the
729 different PVY populations and the virus load at the systemic level was estimated one month post
730 inoculation by quantitative DAS-ELISA as described in Quenouille et al. (2014) (matrices 27 and 28). In
731 addition, the area under the disease progress curve (AUDPC) was calculated using a semi-
732 quantitative scoring scale as in Caranta et al. (1997) (matrices 29 and 30) and the dry weight of
733 infected relative to mock-inoculated plants was estimated as in Montarry et al. (2012) (matrices 31
734 and 32). Matrices 27, 29 and 31 on one side and matrices 28, 30 and 32 on the other side correspond
735 to two independent experiments with slightly different sets of PVY populations.

736

737 *Network analyses*

738 The nestedness and modularity of the different matrices were estimated, and their statistical
739 significance tested respectively with the ‘bipartite’ and ‘igraph’ packages of the R software version
740 3.5.1 (<http://cran.r-project.org/>). These analyses were initially developed for the study of social, then
741 of ecological, networks (or equivalently matrices) containing counts of links between individuals or
742 between interacting species. Hence, to perform these analyses, the matrices should only contain
743 integer values. Moreover, some nestedness or modularity algorithms cannot run in the absence of
744 zero-valued matrix cells or in the presence of an excess of zero-valued cells leading to an
745 unconnected network.

746 Consequently, the first step consisted in transforming the actual matrices accordingly. In all matrices,
747 pathogenicity trait values were transformed into integers from 0 to 9. For this, ten intervals with
748 equal sizes and spanning the range of the pathogenicity trait values of the actual matrix were
749 defined. The bounds of these intervals are $[P_{\min} + (P_{\max} - P_{\min}) * i / 10, P_{\min} + (P_{\max} - P_{\min}) * (i + 1) / 10]$,
750 with i being an integer in the $[0,9]$ interval and P_{\max} and P_{\min} being the maximal and minimal
751 pathogenicity trait values in the whole matrix, respectively. Then, depending on its inclusion in a
752 given pathogenicity trait value interval defined as above, each matrix value was transformed into the
753 corresponding i integer value. When necessary, the matrix was modified in order that grades 0 and 9
754 correspond to the minimal and maximal pathogenicity classes, respectively, and not the opposite. A
755 continuous distribution of the pathogenicity grades was observed in 30 of 32 matrices (Fig. 2).
756 However, for matrices 17b and 22 that contained a large number of zero-values cells, phenotypic
757 values were log-transformed to spread out the data more evenly among the ten phenotypic classes.
758 As these log-transformed matrices produced similar results to the actual matrices in terms of
759 significance of nestedness and modularity, only the latter are shown. To test if the matrices could fit
760 with the inverse-matching-allele model (Fig. 1), we also analyzed the “reverse matrices”, where 0 and
761 9 correspond to the minimal and maximal plant resistance classes, respectively. Methods to estimate
762 nestedness and modularity are detailed in Weitz et al. (2013). Whereas many algorithms can
763 measure the nestedness of matrices containing binary data (0 and 1), only two algorithms were
764 available for matrices containing quantitative numeric data: the weighted nestedness metric based
765 on overlap and decreasing filling (*wNODF* algorithm) (Almeida-Neto et al. 2008) and the weighted-
766 interaction nestedness estimator (*WINE* algorithm) (Galeano et al. 2009). In the R software, the
767 ‘nested’ and ‘wine’ functions were used to estimate the *wNODF* and *WINE* scores, respectively.
768 Because none of the module detection algorithms developed to date provide consistently optimal
769 results in all matrices (Aldecoa and Marín 2013), we used seven different algorithms implemented
770 into the R software (see Supplementary Methods 1 for details). To determine the statistical
771 significance of the patterns (nestedness or modularity) of the plant-parasite interaction matrices, the

772 actual interaction matrices were compared to matrices simulated under several null models
773 (Supplementary Methods 1).

774 As the modularity algorithms (and nestedness algorithms to a lower extent) and null models
775 provided contrasted results (Tables 2 to 4), we used simulations to compare their performances
776 (type I and type II error rates) and help the interpretation of the results (Supplementary Methods 1;
777 Tables S1 to S18).

778 Two modularity algorithms (*walktrap* and *label prop*) provided modularity estimates of 0 (or near 0)
779 for almost all actual matrices and associated null models. Moreover, almost all simulations also
780 provided modularity estimates of 0 with these algorithms, hampering the evaluation of type I and
781 type II error rates (Supplementary Methods 1). Consequently, these two algorithms were not
782 considered for further analyses.

783

784 **Acknowledgements**

785 Marie-Claire Kerlan and Lionel Renault are acknowledged for their help to produce matrix number
786 25 and Anne Massire, Ghislaine Nemouchi, Thérèse Phaly, Bruno Savio and Patrick Signoret for their
787 assistance to produce matrix number 17. We thank Amine Slim from the National Gene Bank of
788 Tunisia (NGBT) for providing seeds of the durum wheat landrace “Mahmoudi Joumine” used to build
789 the matrices 12 and 13, and we thank Aurélie Ducasse and Johann Confais for their help in acquiring
790 phenotypic data on the wheat-*Zymoseptoria tritici* pathosystem found in matrices 14 and 15. We
791 thank Isabelle Demeaux (INRAE, SAVE) for providing technical assistance with the downy
792 mildew/grapevine pathosystem. Anne Quillévéré-Hamard, Gwenola Le Roy and Christophe Le May
793 are acknowledged for having co-supervised, managed and/or significantly contributed to the
794 production of matrices number 19 and 20. We thank Loup Rimbaud and Emmanuel Szadkowski
795 (INRAE, PACA) for their comments on an earlier version of the manuscript and Michel Pitrat (INRAE,
796 PACA) for his help for analyses of matrices 10 and 11. We thank the staff of the INRAE CRB-Leg
797 (<https://www6.paca.inrae.fr/gafl/CRB-Legumes>) who maintained the pepper and melon germplasm
798 collections of the GAFL research unit, and of the INRAE experimental facilities of the Plant Pathology
799 research unit (<https://doi.org/10.15454/8DGF-QF70>), the GAFL experimental unit and the PHENOTIC
800 core facility in Angers (<https://doi.org/10.15454/U2BWFJ>) who ensured the production of the plants
801 and maintenance of plant-growth facilities that allowed us to do this work. We thank the staff of the
802 INRAE experimental facilities of IGEPP for having provided and managed equipment for the
803 experiments.

804

805 **Funding**

806 The research was supported by the French National Research Agency (ANR) programs BIOADAPT
807 (grant no. ANR-12-ADAP-0009-04), ArchiV (grant no. ANR-18-CE32-0004-01), CEDRE (grant no. ANR-
808 05-PADD-05) and PeaMUST (grant no. ANR-11-BTBR-0002), the PROGRAILIVE project (grant
809 RBRE160116CR0530019) funded by the Bretagne region, France and European FEADER grants, the
810 fundings of the Institut Carnot PLANT2PRO and the Comité Interprofessionnel des Vins de Bordeaux
811 (CIVB), the INRAE departments "Santé des Plantes et Environnement" (project APÔGÉ and PhD thesis
812 of Safa Ben Krima) and "Génétique et Amélioration des Plantes", the INRAE métaprogramme SMAcH
813 (Sustainable Management of Crop Health), the French Ministry of Agriculture and Food for projects
814 "Recherche et mise au point de méthodes pour évaluer des résistances variétales durables à des
815 agents pathogènes" (CTPS project C2008-29), "Nouvelles sources de résistance à *Aphis gossypii* chez
816 le melon" (CTPS project C06/02) and "Caractérisation de la virulence de *Podosphaera xanthii*, agent
817 causal de l'oïdium du melon, et développement d'un système de codification des races" (CTPS
818 project C-2012-10). UMR1290 BIOGER benefits from the support of Saclay Plant Sciences-SPS (ANR-
819 17-EUR-0007).

820

821 **Conflict of interest disclosure**

822 The authors of this manuscript declare that they have no financial conflict of interest with the
823 content of this article. Benoît Moury in one of the *Peer Community In Evolutionary Biology*
824 recommenders.

825

Table 1: Datasets used to analyze the structure of quantitative plant-parasite interaction matrices. AUDPC : Area under the disease progress curve.

Matrix number	Parasite	Host plant	Matrix size (host × parasite)	Phenotype	Multiple R ^{2a}	Reference or source
Bacterium						
1	<i>Pseudomonas syringae</i>	<i>Prunus armeniaca</i> (apricot)	20 × 9	Length of flat zone around the inoculation point at the surface of the shoot	0.69	Omriani <i>et al.</i> , unpublished
2	<i>P. syringae</i>	<i>P. armeniaca</i>	20 × 9	Length of flat zone around the inoculation point at the surface of the shoot	0.84	Omriani <i>et al.</i> , unpublished
3	<i>P. syringae</i>	<i>P. armeniaca</i>	20 × 9	Length of browning zone around the inoculation point below the bark of the shoot	0.68	Omriani <i>et al.</i> , unpublished
4	<i>P. syringae</i>	<i>P. armeniaca</i>	20 × 9	Length of browning zone around the inoculation point below the bark of the shoot	0.75	Omriani <i>et al.</i> , unpublished
Fungi						
5	<i>Puccinia hordei</i>	<i>Hordeum vulgare</i> (barley)	12 × 14	Relative latent period	0.84	González <i>et al.</i> , 2012
6	<i>Venturia inaequalis</i>	<i>Malus domestica</i> (apple)	14 × 10	% sporulating leaf area (AUDPC)	0.64	Laloi <i>et al.</i> , 2017
7	<i>V. inaequalis</i>	<i>M. domestica</i>	12 × 14	% sporulating leaf area (AUDPC)	0.49	Caffier <i>et al.</i> , 2016
8	<i>V. inaequalis</i>	<i>M. domestica</i>	8 × 24	% sporulating leaf area	0.71	Caffier <i>et al.</i> , 2014
9	<i>Botrytis cinerea</i>	Tomato ^b	12 × 94	Lesion size on leaves	0.59	Soltis <i>et al.</i> , 2019
10	<i>Podosphaera xanthii</i>	<i>Cucumis melo</i> (melon)	19 × 26	Sporulation surface on leaf disks	0.93	Dogimont <i>et al.</i> , unpublished
11	<i>P. xanthii</i>	<i>C. melo</i>	19 × 31	Sporulation surface on plants	0.94	Dogimont <i>et al.</i> , unpublished
12	<i>Zymoseptoria tritici</i>	<i>Triticum turgidum</i> subsp. <i>durum</i> (durum wheat)	12 × 15	% necrotic leaf area (AUDPC)	0.77	Marcel <i>et al.</i> , unpublished
13	<i>Z. tritici</i>	<i>T. turgidum</i> subsp. <i>durum</i>	12 × 15	% sporulating leaf area (AUDPC)	0.76	Marcel <i>et al.</i> , unpublished
14	<i>Z. tritici</i>	<i>Triticum aestivum</i> (bread wheat)	15 × 98	% necrotic leaf area	0.63	Marcel <i>et al.</i> , unpublished
15	<i>Z. tritici</i>	<i>T. aestivum</i>	15 × 98	% sporulating leaf area	0.63	Marcel <i>et al.</i> , unpublished

Oomycetes						
16	<i>Phytophthora capsici</i>	<i>Capsicum annuum</i> (pepper)	10 × 6	Necrosis length on stem (15 days post inoculation)	0.98	Messaouda <i>et al.</i> , 2015
17	<i>P. capsici</i>	<i>C. annuum</i>	53 × 6	Necrosis length on stem (AUDPC)	0.78	Cantet <i>et al.</i> , unpublished
17b ^c	<i>P. capsici</i>	<i>C. annuum</i>	42 × 6	Necrosis length on stem (AUDPC)	-	Cantet <i>et al.</i> , unpublished
18	<i>Phytophthora infestans</i>	<i>Solanum lycopersicum</i> (tomato), <i>S. pimpinellifolium</i> , <i>S. habrochaites</i> and <i>S. pennellii</i>	8 × 7	Necrosis length on stem (AUDPC)	0.90	Ruellan <i>et al.</i> , unpublished
19	<i>Aphanomyces euteiches</i>	Fabaceae ^d	8 × 35	Root disease severity	0.85	Quillévéré-Hamard <i>et al.</i> , 2018
20	<i>A. euteiches</i>	<i>Pisum sativum</i>	10 × 43	Root disease severity	0.86	Quillévéré-Hamard <i>et al.</i> , 2020
21	<i>Plasmopara viticola</i>	<i>Vitis vinifera</i> (grapevine)	8 × 33	Necrosis on leaves	0.76	Paineau and Delmotte, unpublished
22	<i>P. viticola</i>	<i>V. vinifera</i>	8 × 33	Sporulation on leaves	0.80	Paineau and Delmotte, unpublished
Insect						
23	<i>Aphis gossypii</i>	<i>C. melo</i>	13 × 9	Acceptance of plants	0.61	Boissot <i>et al.</i> , 2016
24	<i>A. gossypii</i>	<i>C. melo</i>	13 × 9	Ability to colonize plants	0.59	Boissot <i>et al.</i> , 2016
Nematode						
25	<i>Globodera pallida</i>	<i>Solanum tuberosum</i> (potato)	10 × 20	Cyst number (relative values)	0.58	Fournet <i>et al.</i> , unpublished
26	<i>G. pallida</i>	Wild potato species	12 × 13	Cyst eclosion rate	0.81	Gautier <i>et al.</i> , 2020
Virus						
27	Potato virus Y (PVY)	<i>C. annuum</i>	7 × 8	Virus load	0.79	Doumayrou <i>et al.</i> , unpublished
28	PVY	<i>C. annuum</i>	9 × 7	Virus load	0.73	Doumayrou <i>et al.</i> , unpublished
29	PVY	<i>C. annuum</i>	8 × 7	Symptom intensity (AUDPC)	0.78	Doumayrou <i>et al.</i> , unpublished
30	PVY	<i>C. annuum</i>	7 × 7	Symptom intensity (AUDPC)	0.81	Doumayrou <i>et al.</i> , unpublished
31	PVY	<i>C. annuum</i>	8 × 7	Relative dry matter weight	0.66	Doumayrou <i>et al.</i> , unpublished
32	PVY	<i>C. annuum</i>	7 × 7	Relative dry matter weight	0.45	Doumayrou <i>et al.</i> , unpublished

^a Fit of the linear model: pathogenicity ~ 'parasite strain' + 'plant accession' (multiple coefficient of determination).

^b Two species: cultivated tomato (*Solanum lycopersicum*) and wild tomato (*S. pimpinellifolium*).

^c Matrix 17b is identical to matrix 17 except that columns entirely made of zero-valued cells and redundant columns were removed.

^d Four species: three pea (*Pisum sativum*) accessions, two vetch (*Vicia sativa*) accessions, two faba bean (*Vicia faba*) accessions and one alfalfa (*Medicago sativa*) accession.

Table 2: Analysis of nestedness of plant-parasite interaction matrices with two methods.

Matrix number	WINE method								wNODF method							
	Nestedness score ^a	Null model ^b							Nestedness score	Null model ^b						
		B	N	C1	R1	S	C2	R2		B	N	C1	R1	S	C2	R2
1	0.78	0 ^c	0	0	0	0	0	0	30.9	0.05	0	0	0	0	0	0
2	0.81	0.01	0	0	0	0	0	0	43.7	0.06	0	0	0	0	0	0
3	0.82	0	0	0	0	0	0	0	47.6	0	0	0	0	0	0	0
4	0.82	0	0	0	0	0	0	0	46.9	0	0	0	0	0	0	0
5	0.83	0	0	0	0	0	0	0	23.2	0.24	0	0.42	0	0	0.36	0
6	0.70	0.12	0	0	0	0	0	0	55.4	0.15	0	0	0	0	0	0
7	0.60	0.49	0	0	0	0	0	0	43.9	0.41	0	0	0	0	0	0
8	0.58	0.01	0	0	0	0	0	0	49.4	0.66	0	0	0	0	0	0
9	0.46	0	0	0	0	0	0	0	42.4	0.01	0	0	0	0	0	0
10	1.01	0	0	0	0	0	0	0	72.7	0	0	0	0	0	0	0
11	1.04	0	0	0	0	0	0	0	75.4	0	0	0	0	0	0	0
12	0.69	0	0	0	0	0	0	0	10.1	0.68	0.85	0.67	1	0.73	0.54	0.90
13	0.73	0	0	0	0	0	0	0	30.0	0.16	0.38	0.48	0.07	0.35	0.39	0.52
14	0.76	0	0	0	0	0	0	0	22.3	0.76	1	1	1	0.06	1	0.22
15	0.68	0.12	0	0	0	0	0	0	41.9	0.31	0	0	0	0	1	0
16	0.84	0	0	0	0	0	0	0	38.6	0.09	0	0	0	0	0	0
17	0.84	0	0	0	0	0	0	0	51.0	0	0	0	0	0	0	0
18	0.93	0	0	0	0	0	0	0	59.2	0	0	0	0	0	0	0
19	0.79	0	0	0	0	0	0	0	9.4	0.89	0.01	0.01	0.80	0.04	0	0.01
20	0.80	0	0	0	0	0	0	0	15.0	0.98	0	0	0	0	0.12	0
21	0.75	0.90	0	0.07	0	0	0.46	0	27.6	0.33	0.42	0.68	0	0.51	1	0.59
22	0.91	0	0	0	0	0	0	0	49.2	0	0	0	0	0	0	0
23	0.75	0	0	0	0	0	0	0.04	6.1	0.65	0.82	0.28	1	0.82	0.48	0.85
24	0.68	0.12	0	0	0.01	0	0	0.02	22.4	0.29	0.98	0.96	0.72	0.95	0.93	0.72
25	0.82	0.01	0	0	0	0	0	0	44.1	0.20	0	0	0	0	0.02	0
26	0.86	0	0	0	0	0	0	0	34.3	0	0	0	0	0	0	0
27	0.69	0.37	0	0	0	0	0	0	51.2	0.41	0	0	0.01	0	0.01	0
28	0.63	0.46	0	0.01	0	0	0	0	58.0	0.27	0	0	0	0	0	0
29	0.78	0.01	0	0	0	0	0	0	22.3	0.97	0.81	0.62	0.02	0.88	0.96	0.18
30	0.84	0.03	0	0	0	0	0	0	66.8	0.01	0	0	0	0	0	0
31	0.77	0	0	0	0	0	0	0.01	21.3	0.05	0.30	0.49	0.04	0.21	0.35	0.06
32	0.52	0.31	0.06	0	0.36	0.06	0.01	0.71	11.1	0.13	0.65	0.55	0.90	0.62	0.51	0.74

^aMean of 100 estimates.

^bSee Supplementary Methods 1 for details of the null models.

^cNestedness significance: the probability value (p-value) indicates the frequency of null-model matrices showing a strictly higher nestedness score than that of the actual matrix. P-values ≤ 0.05 (significant nestedness) are in bold on grey cells and p-values > 0.95 (significant anti-nestedness) are in white on black cells.

Table 3. Analysis of modularity of plant-parasite interaction matrices with the *spinglass* method.

Matrix number	<i>Spinglass</i>								
	Modularity score ^a	Number of modules ^b	Null model ^c						
			B	N	C1	R1	S	C2	R2
1	0.058	-	0.69 ^d	0.76	0.79	0.71	0.93	0.89	0.93
2	0.070	-	0.86	1	1	0.84	1	1	0.92
3	0.084	-	0.32	0.68	0.38	0.42	0.36	0.20	0.22
4	0.095	-	0.95	1	1	0.97	0.99	0.98	0.89
5	0.070	2	0	0	0	0	0	0	0
6	0.102	3	0	0	0	0	0	0	0
7	0.079	-	0.97	1	1	1	0.99	0.96	0.95
8	0.069	-	0.07	0.53	0.35	0.05	0.70	0.66	0.34
9 ^e	0.069	-	0.96	1	1	0.97	0.89	0.97	0.86
10	0.077	3	0	0.07	0	0.03	0.01	0.05	0.04
11	0.086	3	0	0	0	0	0	0	0
12	0.057	-	0.98	0.98	0.99	0.96	1	0.99	0.91
13	0.072	-	0.08	0.27	0.23	0.06	0.73	0.43	0.38
14	0.062	2	0	0	0	0	0	0.01	0
15 ^e	0.079	-	0.06	0.61	0.14	0.68	0.13	0.08	0.39
16	0.078	-	0.20	0.39	0.32	0.37	0.66	0.41	0.86
17 ^b	0.097	3	0.05	0.25	0.15	0.06	0.05	0.01	0.02
18	0.097	-	0.77	0.98	0.97	0.93	0.95	0.71	0.97
19	0.051	-	1	1	1	1	1	1	1
20	0.040	-	1	1	1	1	1	1	1
21	0.092	-	0.44	0.97	0.59	1	0.99	0.56	0.98
22	0.083	-	0.15	NA ^g	0.06	0.44	NA ^g	0.02	0.30
23 ^e	0.072	-	0.41	0.39	0.27	0.36	0.65	0.57	0.54
24	0.063	-	0.30	0.52	0.58	0.27	0.81	0.77	0.53
25	0.091	-	0.75	0.99	0.78	0.99	0.75	0.58	0.45
26 ^e	0.045	-	0.79	0.91	0.86	0.90	1	0.99	1
27	0.130	-	0.73	0.83	0.74	0.85	0.76	0.74	0.89
28	0.090	-	0.96	0.98	0.98	1	0.91	1	0.98
29 ^e	0.078	-	0.89	0.79	0.91	0.79	0.93	1	0.89
30	0.095	-	0.49	0.80	0.82	0.56	0.59	0.58	0.49
31	0.061	-	0.98	1	0.98	1	1	1	0.99
32	0.065	-	1	0.99	1	0.99	0.97	0.97	0.99

^aMaximum of 100 estimates.

^bThe optimal number of modules determined by *spinglass* is indicated only for matrices significantly modular with a majority of null models (Fig. 4).

^cSee Supplementary Methods 1 for details of the null models.

^dModularity significance: the probability value (p-value) indicates the frequency of null-model matrices showing a strictly higher modularity score than that of the actual matrix. P-values ≤ 0.05 (significant modularity) are in bold on grey cells. Significant anti-modularity, when $\leq 5\%$ of null-model matrices show a strictly lower modularity degree than that of the actual matrix, are indicated in white on black cells. Note that some of the indicated p-values are ≥ 0.95 but do not correspond to significant anti-modularity because the modularity degrees of the actual matrix and of some null-model matrices are identical.

^eRows and/or columns entirely made of zero-valued cells were removed since the *spinglass* method cannot estimate the modularity under such circumstances (unconnected graphs).

^fMatrix 17b is identical to matrix 17 except that columns entirely made of zero-valued cells and redundant columns were removed.

^gNA: not available; many null-model matrices had rows and/or columns entirely made of zero-valued cells and the *spinglass* method could not estimate their modularity.

Table 4. Analysis of modularity of plant-parasite interaction matrices with four methods. Only the three null models S, C2 and R2 that provided the lowest rates of false positive modularity in our performance study (Supplementary Methods 1) are presented.

Matrix number	<i>Edge betweenness</i>			<i>Fast greedy</i>			<i>Louvain</i>			<i>Leading eigenvector</i>						
	Modularity score ^a	Null model ^b			Modularity score ^a	Null model ^b			Modularity score ^a	Null model ^b			Modularity score ^a	Null model ^b		
		S	C2	R2		S	C2	R2		S	C2	R2		S	C2	R2
1	0.012	1^c	1	0.99	0.074	1	0.99	0.51	0.073	1	1	1	0.061	0.87	0.77	0.62
2	0.022	1	1	0.97	0.091	1	1	0.98	0.091	1	1	1	0.088	1	1	0.37
3	0.099	0.88	0.53	0.06	0.126	1	0.96	0.38	0.127	1	1	0.64	0.116	0.85	0.62	0.12
4	0	1	1	1	0.113	1	1	1	0.115	1	1	1	0.113	1	1	0.40
5	0.018	1	0.01	1	0.065	0.99	0	0.99	0.069	1	0	1	0.069	0.58	0	0.57
6	0.085	1	0.99	1	0.209	0.88	0.03	0.17	0.209	0.96	0.10	0.42	0.206	0.50	0.01	0.07
7	0.138	0.96	0.45	0.79	0.240	1	0.84	1	0.240	1	0.98	1	0.160	1	0.97	0.99
8	0.003	1	1	1	0.121	1	1	0.98	0.125	1	1	1	0.116	0.99	0.97	0.43
9	0	1	1	1	0.074	1	1	1	0.069	1	1	1	0.061	0.99	0.84	0.59
10	0	1	1	1	0.073	1	1	1	0.073	1	0.98	1	0.072	1	0.40	0.47
11	0	1	1	1	0.085	1	0.98	1	0.091	1	0.93	1	0.058	1	0.96	0.99
12	0.004	1	1	0.50	0.041	1	1	0.16	0.044	1	1	0.98	NA ^c	NA ^d	NA ^d	NA ^d
13	0.004	1	1	0.95	0.061	1	1	0.56	0.063	1	1	0.88	0.039	0.96	0.94	0.64
14	0	1	1	1	0.044	0.87	0.04	0.35	0.046	0.48	0.04	0.15	0.010	1	0.41	1
15	0	1	1	1	0.089	1	0.98	1	0.087	1	1	1	0.063	0.99	0.64	1
16	0.007	1	1	1	0.032	1	1	1	0.036	1	1	1	0.022	0.99	0.92	1
17	0.071	1	0.99	1	0.172	1	1	1	0.177	1	1	1	0.155	1	0.99	0.99
17b ^e	0.040	1	1	0.99	0.155	1	1	1	0.158	1	1	1	0.131	0.38	0.21	0.96
18	0.079	1	1	1	0.186	1	1	0.35	0.186	0.99	1	0.16	0.169	0.98	1	0.32
19	0	1	1	1	0.028	1	1	1	0.031	1	1	1	0	1	1	1
20	0	1	1	1	0.029	1	1	1	0.029	1	1	1	0.029	0.97	0.88	0.83
21	0.036	1	0.23	1	0.110	1	0	1	0.109	1	0.01	1	0.096	0.99	0	1
22	0.020	1	0.98	1	0.165	1	0.89	1	0.165	1	0.93	1	0.157	1	0.27	1
23	0.011	1	1	0.88	0.068	0.91	0.81	0.22	0.070	0.99	0.99	0.70	0.058	0.67	0.44	0.26
24	0.035	0.99	0.86	0.91	0.092	0.79	0.75	0.20	0.095	0.94	0.93	0.60	0.066	0.90	0.82	0.74
25	0.066	1	0.35	1	0.167	1	0.49	1	0.168	1	0.84	1	0.118	1	0.78	1
26	0	1	1	1	0.041	1	1	1	0.046	1	1	1	0.044	0.82	0.39	0.84
27	0.034	0.96	0.86	0.69	0.102	1	1	1	0.103	1	1	1	0.086	1	1	1
28	0	1	1	1	0.151	1	1	1	0.153	1	1	1	0.108	1	1	1
29	0.008	1	1	1	0.069	1	1	1	0.069	1	1	1	0.048	1	0.95	1
30	0.043	0.98	0.91	0.91	0.087	1	1	1	0.092	1	1	1	0	1	1	1
31	0.013	0.98	0.97	0.65	0.062	1	1	0.89	0.062	1	1	1	0.055	0.69	0.71	0.59
32	0.058	0.70	0.84	0.72	0.062	0.95	0.99	0.59	0.062	1	1	1	0.022	0.97	0.96	0.73

^aMaximum of 100 estimates.

^bSee Supplementary Methods 1 for details of the null models.

^cModularity significance: the probability value (p-value) indicates the frequency of null-model matrices showing a strictly higher modularity score than that of the actual matrix. P-values ≤ 0.05 (significant modularity) are in bold on grey cells. Significant anti-modularity, when $\leq 5\%$ of null-model matrices show a strictly lower modularity degree than that of the actual matrix, are indicated in white on black cells. Note that some of the indicated p-values are ≥ 0.95 but do not correspond to significant anti-modularity because the modularity degrees of the actual matrix and of some null-model matrices are identical.

^dNA: not available; the *leading eigenvector* algorithm failed to converge.

^eMatrix 17b is identical to matrix 17 except that columns entirely made of zero-valued cells and redundant columns were removed.

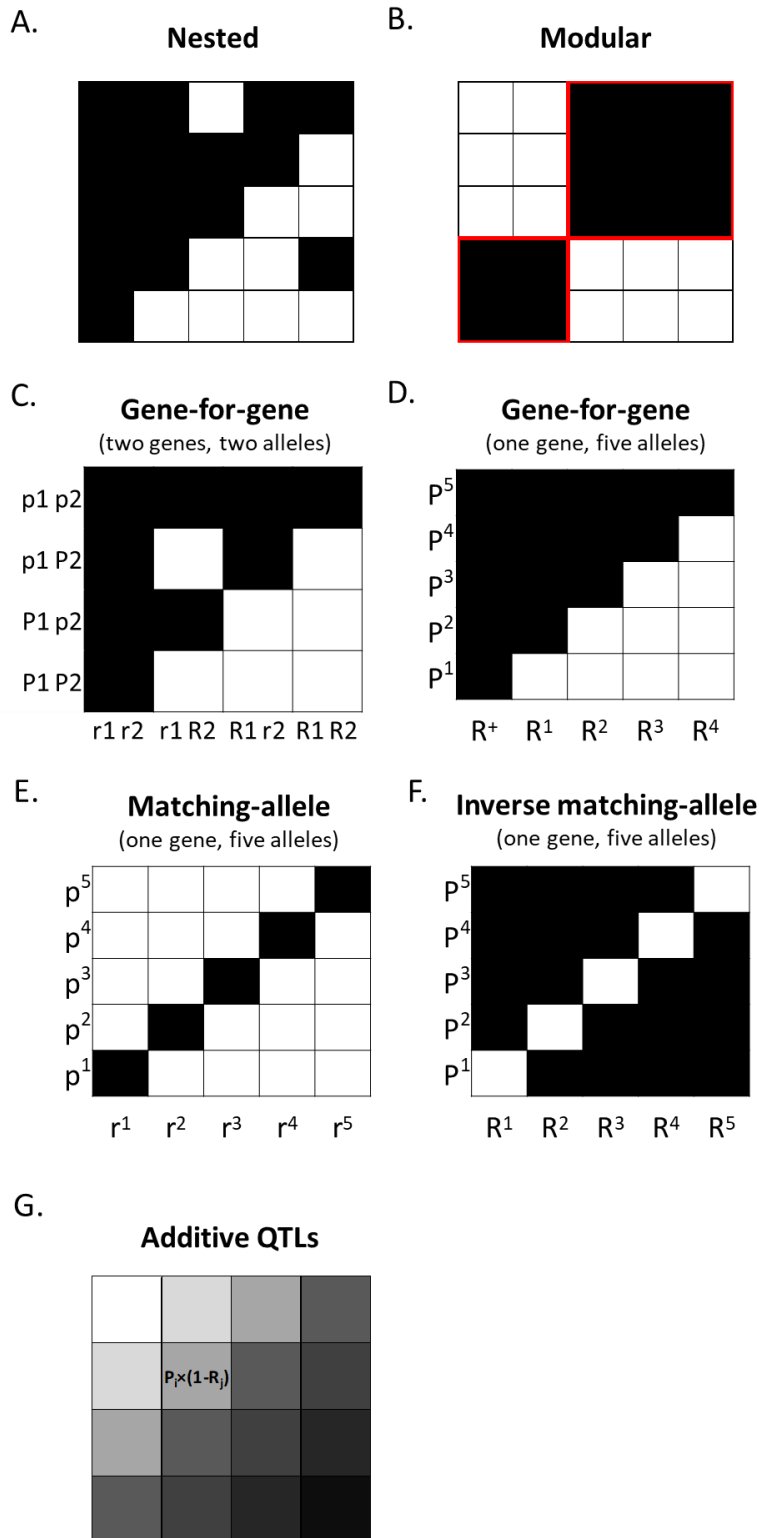


Figure 1. Matrices corresponding to different mechanistic, genetic and evolutionary models of qualitative or quantitative host-parasite interactions. In each case, host genotypes correspond to different columns and parasite genotypes to different rows) and black and white cells (or 1 and 0 grades) correspond to infection or lack of infection, respectively. A: Illustration of an imperfectly nested pattern. B: Illustration of a perfectly modular pattern (modules are delimited with red lines). C and D: Gene-for-gene (GFG) models with partial or perfectly nested patterns. C: Case of two genes with two alleles in both hosts and parasites. Infection occurs only when no elicitor in the

parasite is recognized by a product of the resistance alleles in the host. In the other situations, resistance is induced and there is no infection. D: Case of a single gene with five alleles in both hosts and parasites. Resistance alleles have various levels of specificity: in some plant accessions resistance can be induced by several parasite strains. E: Matching-allele model. Infection occurs only if the product of the pathogenicity allele is recognized by the product of the susceptibility allele in the host. F: Variation of D with higher specificity: resistance is induced by a specific product present in a single parasite genotype. This model was named "inverse matching-allele" model (Thrall et al. 2016) and has an anti-modular structural pattern. G: Additive QTL model with no plant-parasite QTL \times QTL interaction. For each parasite strain i with pathogenicity level P_i and each plant accession j with resistance level R_j , infection score corresponds to $P_i \times (1-R_j)$.

Superscript figures correspond to alleles of a given gene whereas normal font figures correspond to different genes. Matching genes or alleles at resistance and pathogenicity loci in host and parasite genotypes share the same figure. For simplicity, hosts and parasites are considered haploid. R: resistance allele; r or R⁺: susceptibility allele; P: allele controlling lack of pathogenicity; p: pathogenicity allele.

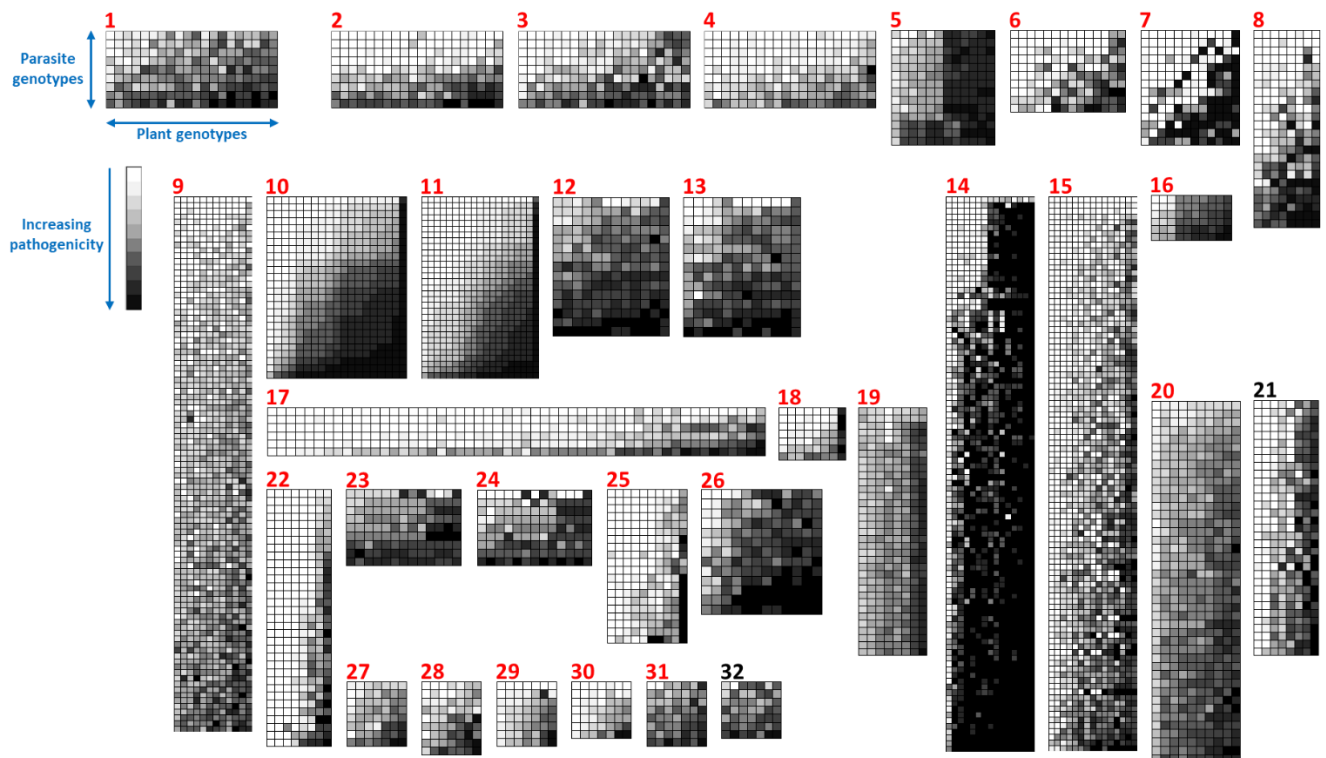


Figure 2. Overview of the 32 analyzed plant-parasite matrices (Table 1). Different plant accessions and parasite strains correspond to different columns and rows, respectively. White to black shades in each cell correspond to an increasing gradient of pathogenicity or infectivity (corresponding to 0 to 9 values in the analysed matrices) for a given plant and parasite pair. Rows and columns were ordered by increasing marginal totals, revealing the nested patterns. Red numbers correspond to significant nestedness (*WINE* algorithm) (Table 2).

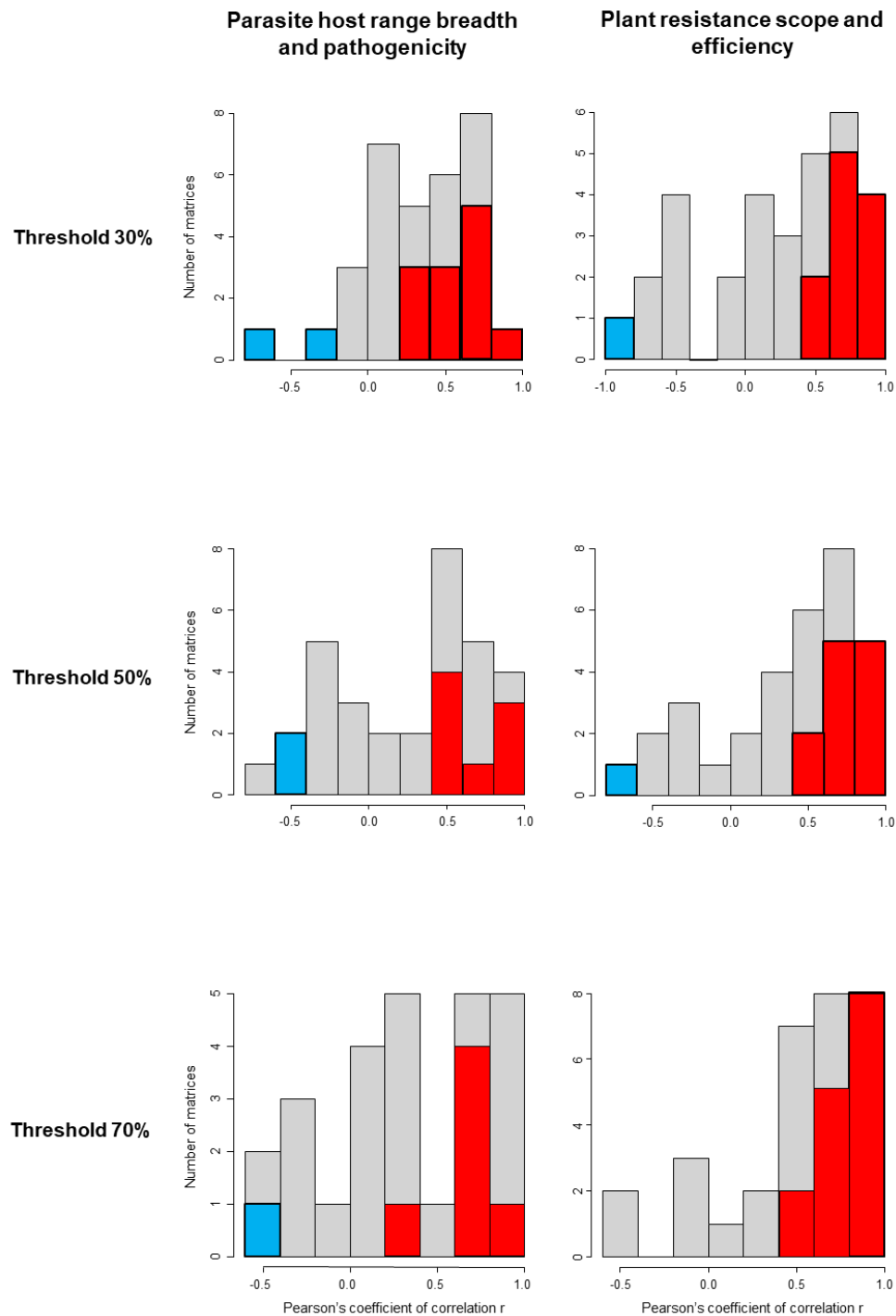


Figure 3. Distributions of Pearson's coefficients of correlation (r) between parasites host range breadth and pathogenicity (left) or between plant resistance efficiency and scope (right) across the 32 analysed matrices for different thresholds separating hosts and non-hosts (or parasites included or not included in the resistance scope). Each threshold corresponds to a percentage of the maximal pathogenicity value in each matrix (only results obtained with thresholds corresponding to 30%, 50% and 70% of the maximal pathogenicity value are shown; results were similar for other thresholds). In blue and red: significantly negative or positive r values (p -value < 0.05). For some thresholds and some matrices, the coefficient of correlation could not be calculated because too few pathogenicity data remained.

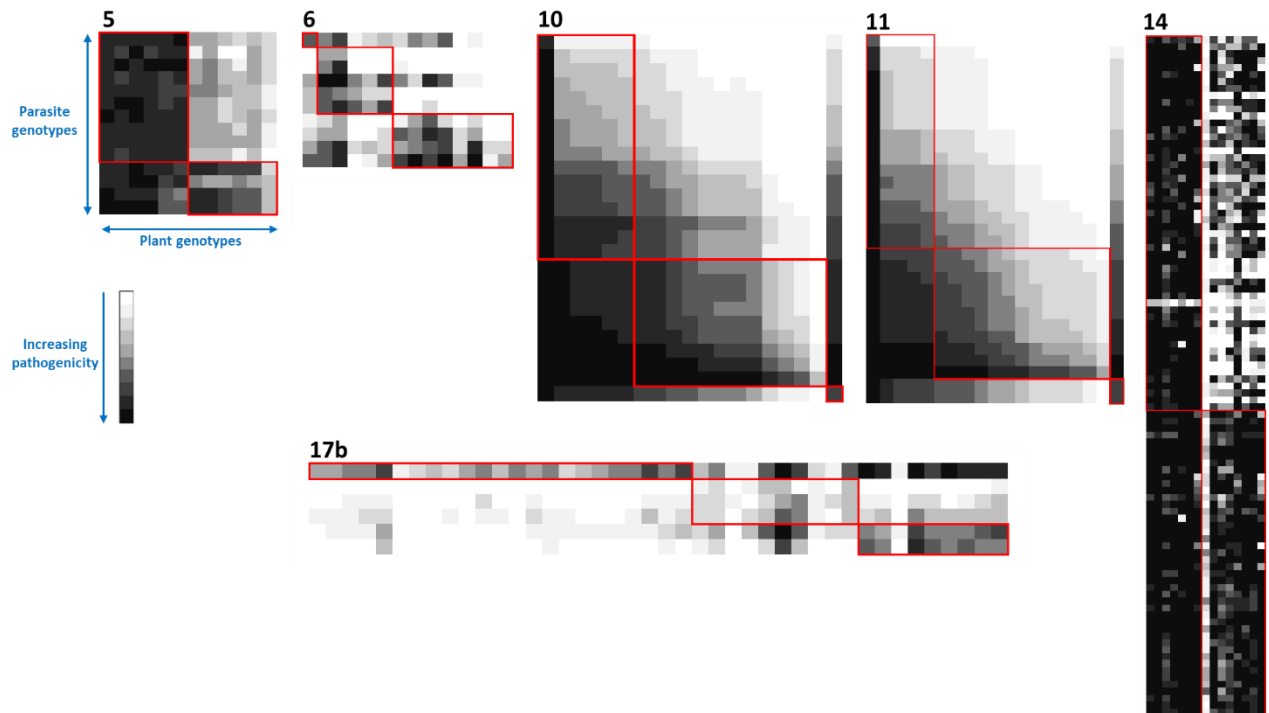


Figure 4. Overview of the six plant-parasite matrices showing significant modularity with the *spinglass* algorithm (Table 3). Rows and columns were ordered by modules, delimited by red lines. See legend of Figure 2 for the representation of matrices.

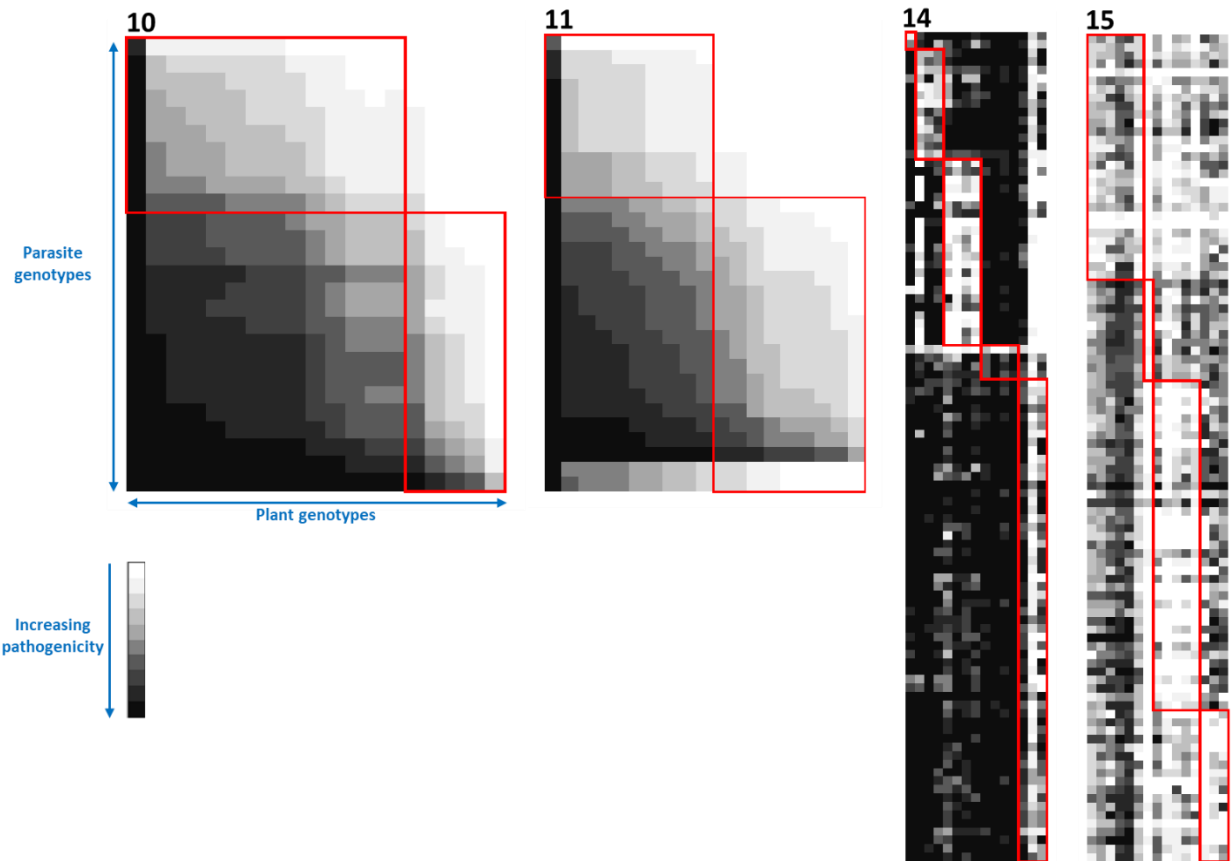


Figure 5. Overview of the four plant-parasite matrices showing significant modularity with the *spinglass* algorithm when matrices were transformed such that 0 values correspond to the maximal plant susceptibility and 9 values to the maximal plant resistance (but note that the matrices are represented such that 0 to 9 values correspond to a plant resistance to susceptibility gradient, as in the original matrices). Rows and columns were ordered by modules, delimited by red lines. See legend of Figure 2 for the representation of matrices.

References

- Aldecoa, R., Marín, I. 2013. Exploring the limits of community detection strategies in complex networks. *Sci. Rep.* 3:2216.
- Almeida-Neto, M., Ulrich, W. 2011. A straightforward computational approach for measuring nestedness using quantitative matrices. *Environ. Model. Softw.* 26:173-176.
- Almeida-Neto, M., Guimaraes, P., Guimaraes, P.R., Loyola, R.D., Ulrich, W. 2008. A consistent metric for nestedness analysis in ecological systems: reconciling concept and measurement. *Oikos* 117:1227–1239.
- Bahri, B., Kaltz, O., Leconte, M., de Vallavieille-Pope, C., Enjalbert, J. 2009. Tracking costs of virulence in natural populations of the wheat pathogen, *Puccinia striiformis f.sp.tritici*. *BMC Evol. Biol.* 9:26.
- Bartoli, C., Roux, F. 2017. Genome-wide association studies in plant pathosystems: Toward an ecological genomics approach. *Front. Plant Sci.* 8:763.
- Ben Krima, S., Slim, A., Gelisse, S., Kouki, H., Nadaud, I., Sourdille, P., Yahyaoui, A., Ben M'barek, S., Suffert, F., Marcel, T.C. 2020. Life story of Tunisian durum wheat landraces revealed by their genetic and phenotypic diversity. *bioRxiv* 2020.08.14.251157.
- Barrett, L.G., Encinas-Viso, F., Burdon, J.J., Thrall, P.H. 2015. Specialization for resistance in wild host-pathogen interaction networks. *Front. Plant Sci.* 6:761.
- Bascompte, J., Jordano, P., Melián, C.J., Olesen, J.M. 2003. The nested assembly of plant–animal mutualistic networks. *Proc. Natl. Acad. Sci. USA* 100:9383–9387.
- Bent, A. F., Mackey D. 2007. Elicitors, effectors, and R genes: the new paradigm and a lifetime supply of questions. *Annu. Rev. Phytopathol.* 45:399-436.
- Blondel, V.D., Guillaume, J.-L., Lambiotte, R., Lefebvre, E. 2008. Fast unfolding of communities in large networks. *J. Stat. Mech.: Theory Exp.* 10:P10008.
- Boissot, N., Thomas, S., Chovelon, V., Lecoq, H. 2016. NBS-LRR-mediated resistance triggered by aphids: viruses do not adapt; aphids adapt via different mechanisms. *BMC Plant Biol.* 16:25.
- Brown J.K.M. 2015. Durable resistance of crops to disease: a Darwinian perspective. *Annu. Rev. Phytopathol.* 53:513-539.
- Brualdi, R.A., Sanderson, J.G. 1999. Nested species subsets, gaps, and discrepancy. *Oecologia* 119:256-264.
- Bruns, E., Carson, M., May, G. 2014. The Jack of all trades is master of none: a pathogen's ability to infect a greater number of host genotypes comes at a cost of delayed reproduction. *Evolution* 68:2453-2466.
- Caffier, V., Didelot, F., Pumo, B., Causeur, D., Durel, C.E., Parisi, L. 2010. Aggressiveness of eight *Venturia inaequalis* isolates virulent or avirulent to the major resistance gene *Rvi6* on a non-*Rvi6* apple cultivar. *Plant Pathol.* 59:1072-1080.
- Caffier, V., Lasserre-Zuber, P., Giraud, M., Lascostes, M., Stievenard, R., Lemarquand, A., Van De Weg, E., Expert, P., Denancé, C., Didelot, F., Le Cam, B., Durel, C.E. 2014. Erosion of quantitative host resistance in the apple - *Venturia inaequalis* pathosystem. *Infect. Genet. Evol.* 27:481-489.
- Caffier, V., Le Cam, B., Al Rifai, M., Bellanger, M.N., Comby, M., Denancé, C., Didelot, F., Expert, P., Kerdraon, T., Lemarquand, A., Ravon, E., Durel, C.E. 2016. Slow erosion of a quantitative apple

- resistance to *Venturia inaequalis* based on an isolate-specific Quantitative Trait Locus. *Infect. Genet. Evol.* 44:541-548.
- Caranta, C., Lefebvre, V., Palloix, A. 1997. Polygenic resistance of pepper to potyviruses consists of a combination of isolate-specific and broad-spectrum quantitative trait loci. *Mol. Plant-Microbe Interact.* 10:872–878.
- Castagnone-Sereno, P., Bongiovanni, M., Wajnberg E. 2007. Selection and parasite evolution: A reproductive fitness cost associated with virulence in the parthenogenetic nematode *Meloidogyne incognita*. *Evol. Ecol.* 21:259-270.
- Clauset, A., Newman, M.E.J., Moore, C. 2004. Finding community structure in very large networks. *Phys. Rev. E* 70:066111.
- Danan, S., Chauvin, J.-E., Caromel, B., Moal, J.-D., Pellé, R., Lefebvre, V. 2009. Major-effect QTLs for stem and foliage resistance to late blight in the wild potato relatives *Solanum sparsipilum* and *S. spegazzinii* are mapped to chromosome X. *Theor. Appl. Genet.* 119:705–719.
- Delmas, C.E.L., Fabre, F., Jolivet, J., Mazet, I.D., Cervera, S.R., Delière, L., Delmotte F. 2016. Adaptation of a plant pathogen to partial host resistance: selection for greater aggressiveness in grapevine downy mildew. *Evol. Appl.* 9:709–725.
- Desbiez, C., Gal-On, A., Girard, M., Wipf-Scheibel, C., Lecoq, H. 2003. Increase in *Zucchini yellow mosaic virus* symptom severity in tolerant zucchini cultivars is related to a point mutation in P3 protein and is associated with a loss of relative fitness on susceptible plants. *Phytopathology* 93:1478-1484.
- Dormann, C.F., Fründ, J., Schaefer, H.M. 2017. Identifying causes of patterns in ecological networks: Opportunities and limitations. *Annu. Rev. Ecol. Evol. Syst.* 48:559-584.
- Feng, W, Takemoto, K. 2014. Heterogeneity in ecological mutualistic networks dominantly determines community stability. *Sci. Rep.* 4:5912.
- Fenton, A., Antonovics, J., Brockhurst, M.A. 2009. Inverse-gene-for-gene infection genetics and coevolutionary dynamics. *Am. Nat.* 174:E230-E242.
- Flor, H.H. 1956. The complementary genic systems in flax and flax rust. *Adv. Genet.* 8:29–54.
- Flores, C.O., Meyer, J.R., Valverde, S., Farr, L., Weitz, J.S. 2011. Statistical structure of host-phage interactions. *Proc. Natl. Acad. Sci. USA* 108: E288–97.
- Flores, C.O., Valverde, S., Weitz, J.S. 2013. Multi-scale structure and geographic drivers of cross-infection within marine bacteria and phages. *ISME J.* 7:520-532.
- Fortuna, M.A., Barbour, M.A., Zaman, L., Hall, A.R., Buckling, A., Bascompte, J. 2019. Coevolutionary dynamics shape the structure of bacteria–phage infection networks. *Evolution* 73:1001–1011.
- Fournet, S., Eoche-Bosy, D., Renault, L., Hamelin, F.M., Montarry, J. 2016. Adaptation to resistant hosts increases fitness on susceptible hosts in the plant parasitic nematode *Globodera pallida*. *Ecol. Evol.* 6:2559-2568.
- Fraile, A., Pagán, I., Anastasio, G., Saez, E., García-Arenal, F. 2011. Rapid genetic diversification and high fitness penalties associated with pathogenicity evolution in a plant virus. *Mol. Biol. Evol.* 28:1425-1437.
- Galeano, J., Pastor, J.M., Iriando, J.M. 2009. Weighted-Interaction Nestedness Estimator (WINE): A new estimator to calculate over frequency matrices. *Env. Model. Soft.* 24:1342-1346.

- Gallois, J.-L., Moury, B., German-Retana, S. 2018. Role of the genetic background in resistance to plant viruses. *Int. J. Mol. Sci.* 19:2856.
- Gautier, C., Fournet, S., Piriou, C., Renault, L., Yvin, J.C., Nguema-Ona, E., Grenier, E., Montarry, J. 2020. Plant-parasite coevolution: a weak signature of local adaptation between Peruvian *Globodera pallida* populations and wild potatoes. *Ecol. Evol.* 10:4156-4163.
- González, A.M., Marcel, T.C., Niks, R.E. 2012. Evidence for a minor gene-for-minor gene interaction explaining nonhypersensitive polygenic partial disease resistance. *Phytopathology* 102:1086-1093.
- Gotelli, N.J., Graves, G.R. 1996. Null models in ecology. Smithsonian Institution Press, Washington D.C.
- Grosberg, R.K., Hart, M.W. 2000. Mate selection and the evolution of highly polymorphic self/nonself recognition genes. *Science* 289:2111-2114.
- Huang, Y.J., Balesdent, M.-H., Li, Z.Q., Evans, N., Rouxel, T., Fitt, B.D.L. 2010. Fitness cost of virulence differs between the *AvrLm1* and *AvrLm4* loci in *Leptosphaeria maculans* (phoma stem canker of oilseed rape). *Eur. J. Plant Pathol.* 126:279-291.
- Ishibashi, K., Mawatari, N., Miyashita, S., Kishino, H., Meshi, T., Ishikawa, M. 2012. Coevolution and hierarchical interactions of *Tomato mosaic virus* and the resistance gene *Tm-1*. *PLoS Pathog.* 8:e1002975.
- Janzac, B., Montarry, J., Palloix, A., Navaud, O., Moury, B. 2010. A point mutation in the polymerase of *Potato virus Y* confers virulence towards the *Pvr4* resistance of pepper and a high competitiveness cost in susceptible cultivar. *Mol. Plant-Microbe Interact.* 23:823-830.
- Jenner, C.E., Wang, X.W., Ponz, F., Walsh, J.A. 2002. A fitness cost for *Turnip mosaic virus* to overcome host resistance. *Virus Res.* 86:1-6.
- Jonhson, S., Domínguez-García, V., Muñoz, M.A. 2013. Factors determining nestedness in complex networks. *PLOS ONE* 8:e74025.
- Joppa, L.N., Montoya, J.M., Solé, R., Sanderson, J., Pimm, S.L. 2010. On nestedness in ecological networks. *Ecol. Evol. Res.* 12:35-46.
- Khatabi, B., Wen, R.H., Hajimorad, M.R. 2013. Fitness penalty in susceptible host is associated with virulence of *Soybean mosaic virus* on *Rsv1*-genotype soybean: a consequence of perturbation of HC-Pro and not P3. *Mol. Plant Pathol.* 14:885-897.
- Kidner, J., Moritz, R.A.F. 2013. The Red Queen process does not select for high recombination rates in haplodiploid hosts. *Evol. Biol.* 40:377-84.
- Laloi, G., Vergne, E., Durel, C.-E., Le Cam, B., Caffier, V. 2017. Efficiency of pyramiding of three quantitative resistance loci to apple scab. *Plant Pathol.* 66:412-422.
- Lambrechts, L. 2010. Dissecting the genetic architecture of host-pathogen specificity. *PLoS Pathog.* 6:e1001019.
- Leach, J.E., Vera Cruz, C.M., Bai, J.F., Leung, H. 2001. Pathogen fitness penalty as a predictor of durability of disease resistance genes. *Annu. Rev. Phytopathol.* 39:187-224.
- Lefebvre, V., Palloix, A. 1996. Both epistatic and additive effects of QTLs are involved in polygenic induced resistance to disease: a case study the interaction pepper-*Phytophthora capsici* Leonian. *Theor. Appl. Genet.* 93:503-511.

- Marcel, T.C., Gorguet, B., Truong Ta, M., Kohutova, Z., Vels, A., Niks, R.E. 2008. Isolate specificity of quantitative trait loci for partial resistance of barley to *Puccinia hordei* confirmed in mapping populations and near-isogenic lines. *New Phytol.* 177:743-755.
- Messaouda, B., Guechi, A., Mézaache-Aichour, S. 2015. Susceptibility of Algerian pepper cultivars (*Capsicum annuum* L.) to *Phytophthora capsici* strains from different geographic areas. *Afr. J. Biotechnol.* 14:3011-3018.
- Montarry, J., Hamelin, F.M., Glais, I., Corbière, R., Andrivon, D. 2010. Fitness costs associated with unnecessary virulence factors and life history traits: evolutionary insights from the potato late blight pathogen *Phytophthora infestans*. *BMC Evol. Biol.* 10:283.
- Montarry, J., Cartier, E., Jacquemond, M., Palloix, A., Moury, B. 2012. Virus adaptation to quantitative plant resistance: erosion or breakdown? *J. Evol. Biol.* 25:2242–2252.
- Morris, C.E., Moury, B. 2019. Revisiting the concept of host range of plant pathogens. *Annu. Rev. Phytopathol.* 57:63–90.
- Morris, C.E., Lamichhane, J.R., Nikolić, I., Stanković S., Moury, B. 2019. The overlapping continuum of host range among strains in the *Pseudomonas syringae* complex. *Phytopathology Research* 1:4.
- Morris, C.E., Glaux, C., Latour, X., Gardan, L., Samson, R., Pitrat, M. 2000. The relationship of host range, physiology and genotype to virulence on cantaloupe in *Pseudomonas syringae* from cantaloupe blight epidemics in France. *Phytopathology* 90:636-646.
- Morris CE, Sands DC, Vanneste JL, Montarry J, Oakley B, Guilbaud C, Glaux C (2010). Inferring the evolutionary history of the plant pathogen *Pseudomonas syringae* from its biogeography in headwaters of rivers in North America, Europe and New Zealand. *mBio* 1: e00107-10.
- Newman, M.E.J. 2006. Finding community structure using the eigenvectors of matrices. *Phys. Rev. E* 74:036104.
- Newman M.E.J., Girvan, M. 2004. Finding and evaluating community structure in networks. *Phys. Rev. E* 69:026113.
- Nicot, P.C., Bardin, M., Dik, A.J. 2002. Basic methods for epidemiological studies of powdery mildew: Culture and preservation of isolates, production and delivery of inoculum, and disease assessment. Pages 83-99 in: *The Powdery Mildews: A Comprehensive Treatise*. R. R. Bélanger, W. R. Bushnell, A. J. Dik, and T. L. W. Carver, eds. The American Phytopathological Society, St. Paul, MN.
- Parisi, L., Morgaint, B., Blanco Garcia, J., Guilbaud, C., Chandeysson, C., Bourgeay, J.-F., Moronville, A., Brun, L., Brachet M.-L., Morris, C.E. 2019. Bacteria from four phylogroups of the *Pseudomonas syringae* complex can cause bacterial canker of apricot. *Plant Pathol.* 68:1249-1258.
- Parlevliet, J. E. 1977. Evidence of differential interaction in the polygenic *Hordeum vulgare* - *Puccinia hordei* relation during epidemic development. *Phytopathology* 67:776-778.
- Patefield, W.M. 1981. Algorithm AS159. An efficient method of generating r x c tables with given row and column totals. *J. Royal Stat. Soc.* 30:91–97.
- Perchepied, L., Bardin, M., Dogimont, C., Pitrat, M. 2005. Relationship between loci conferring downy mildew and powdery mildew resistance in melon assessed by quantitative trait loci mapping. *Phytopathology* 95:556-565.
- Peters, A.R., Zhang, Z., Richards, J.K., Friesen, T.L., Faris, J.D. 2019. Genetics of variable disease expression conferred by inverse gene-for-gene interactions in the wheat-*Parastagonospora nodorum* pathosystem. *Plant Physiol.* 180:420-434.

- Pons, P., Latapy, M. 2006. Computing communities in large networks using random walks. *J. Graph Algorithms Appl.* 10:191–218.
- Poulicard, N., Pinel-Galzi, A., Hébrard, E., Fargette, D. 2010. Why *Rice yellow mottle virus*, a rapidly evolving RNA plant virus, is not efficient at breaking *rymv1-2* resistance? *Mol. Plant Pathol.* 11:145–154.
- Quenouille, J., Paulhiac, E., Moury, B., Palloix, A. 2014. Quantitative trait loci from the host genetic background modulate the durability of a resistance gene: a rational basis for sustainable resistance breeding in plants. *Heredity* 112:579–587.
- Quillévéré-Hamard, A., Le Roy, G., Moussart, A., Baranger, A., Andrivon, D., Pilet-Nayel, M.-L., Le May, C. 2018. Genetic and pathogenicity diversity of *Aphanomyces euteiches* populations from pea-growing regions in France. *Front. Plant Sci.* 9:1673.
- Quillévéré-Hamard, A., Le Roy, G., Lesné, A., Le May, C., Pilet-Nayel, M.-L. 2020. Aggressiveness of diverse French *Aphanomyces euteiches* isolates on pea Near-Isogenic-Lines differing in resistance QTL. *Phytopathology*, doi: 10.1094/PHTO-04-20-0147-R.
- Raghavan, U.N., Albert, R., Kumara, S. 2007. Near linear time algorithm to detect community structures in large-scale networks. *Phys. Rev. E* 76:036106.
- Reichardt, J., Bornholdt, S. 2006. Statistical mechanics of community detection. *Phys. Rev. E* 74:016110.
- Sacristán, S., García-Arenal, F. 2008. The evolution of virulence and pathogenicity in plant pathogen populations. *Mol. Plant Pathol.* 9:369–384.
- Saintenac, C., Lee, W.-S., Cambon, F., Rudd, J.J., King, R.C., Marande, W., Powers, S.J., Bergès, H., Phillips, A.L., Uauy, C., Hammond-Kosack, K.E., Langin, T., Kanyuka, K. 2018. Wheat receptor-kinase-like protein *Stb6* controls gene-for-gene resistance to fungal pathogen *Zymoseptoria tritici*. *Nat. Genet.* 50:368–374.
- Soltis, N.E., Atwell, S., Shi, G., Fordyce, R., Gwinner, R., Gao, D., Shafi, A., Kliebenstein D.J. 2019. Interactions of tomato and *Botrytis cinerea* genetic diversity: Parsing the contributions of host differentiation, domestication, and pathogen variation. *Plant Cell* 31:502–519.
- Staniczenko, P.P.A., Kopp, J.C., Allesina, S. 2013. The ghost of nestedness in ecological networks. *Nat. Commun.* 4:1391.
- Suweis, S., Simini, F., Banavar, J.R., Maritan, A. 2013. Emergence of structural and dynamical properties of ecological mutualistic networks. *Nature* 500:449–452.
- Tellier, A., Brown, J.K.M. 2011. Spatial heterogeneity, frequency-dependent selection and polymorphism in host-parasite interactions. *BMC Evol. Biol.* 11:319.
- Thrall, P.H., Barrett, L.G., Dodds, P.N., Burdon, J.J. 2016. Epidemiological and evolutionary outcomes in gene-for-gene and matching allele models. *Front. Plant Sci.* 6:1084.
- Traag, V.A., Bruggeman, J. 2009. Community detection in networks with positive and negative links. *Phys. Rev. E* 80:036115.
- Valverde, S., Elena, S.F., Solé, R. 2017. Spatially induced nestedness in a neutral model of phage-bacteria networks. *Virus Evol.* 3:vex021.
- Valverde, S., Jordi Piñero, J., Corominas-Murtra, B., Montoya, J., Joppa, L., Solé, R. 2018. The architecture of mutualistic networks as an evolutionary spandrel. *Nat. Ecol. Evol.* 2:94–99.

- Vera Cruz, C.M., Bai, J.F., Ona, I., Leung, H., Nelson, R.J., Mew, T.W., Leach J.E. 2000. Predicting durability of a disease resistance gene based on an assessment of the fitness loss and epidemiological consequences of avirulence gene mutation. *Proc. Natl. Acad. Sci. USA* 97:13500-13505.
- Wang, M., Roux, F., Bartoli, C., Huard-Chauveau, C., Meyer, C., Lee, H., Roby, D., McPeck, M.S., Bergelson, J. 2018. Two-way mixed-effects methods for joint association analysis using both host and pathogen genomes. *Proc. Natl. Acad. Sci. USA* 115:E5440-E5449.
- Weitz, J.S., Poisot, T., Meyer, J.R., Flores, C.O., Valverde, S., Sullivan, M.B., Hochberg, M.E. 2013. Phage–bacteria infection networks. *Trends Microbiol.* 21:82–91.
- Wichmann, G., Bergelson, J. 2004. Effector genes of *Xanthomonas axonopodis* pv. *vesicatoria* promote transmission and enhance other fitness traits in the field. *Genetics* 166:693-706.
- Zhong, Z., Marcel, T.C., Hartmann, F.E., Ma, X., Plissonneau, C., Zala, M., Ducasse, A., Confais, J., Compain, J., Lapalu, N., Amselem, J., McDonald, B.A., Croll, D., Palma-Guerrero, J.C. 2017. A small secreted protein in *Zymoseptoria tritici* is responsible for avirulence on wheat cultivars carrying the *Stb6* resistance gene. *New Phytol.* 214:619-631.